ASSESSMENT OF FLOW EFFICIENCY THROUGH A CLOSED CIRCUIT WIND TUNNEL WITH RECOMMENDATIONS FOR IMPROVEMENTS

A Thesis

by

JOHN MARK GUTHERY

Submitted to the Office of Graduate and Professional Studies of
Texas A&M University
in partial fulfillment of the requirements for the degree of

MASTER OF SCIENCE

Chair of Committee,	Edward White
Committee Members,	Othon Rediniotis
	Eric Petersen
Head of Department,	Rodney Bowersox

December 2013

Major Subject: Aerospace Engineering

ABSTRACT

Wind tunnels are designed for a certain range of test velocities and model sizes. The Oran W. Nicks Low Speed Wind Tunnel (LSWT) at Texas A&M, was designed to reach 200 mph (M=0.26) with its original 1250 hp motor and 7 x 10 ft test section. In 2012 the motor and main bearing were replaced with a new 3000 hp motor. With the increased power and motor efficiencies, the tunnel could potentially reach M=0.42 flow. However, the current structure still limits the testing speed to M=0.26. This thesis outlines modifications that may allow the LSWT to reach M=0.5 for testing and potentially M=0.8 for an empty test section. The flow throughout the circuit and concomitant losses will be investigated. Methods for improving the efficiency will be presented, along with their estimated reduction in power loss. In order to reach this higher velocity, a 6 x 5 ft reduced test section with higher structural strength is required. This reduction in test section size requires subsequent diffuser and contraction alterations. The method for designing the diffuser will be presented, along with the design chosen. With these modifications to the tunnel, as well as using estimations of the motor efficiency, and results from measured and estimated losses in the circuit, the testing speed of M=0.5 in an empty test section could be reached with 1,200 to 1,800 hp supplied to the motor.

DEDICATION

For Grandad, who stimulated my interest in all things aerospace. For my family, who played an integral part in making me who I am today. For Nina, who has always offered unwavering support and love.

ACKNOWLEDGEMENTS

I would like to thank my adviser, Dr. Ed White, for his continued support and guidance through this work. I would also like to thank my committee members, Drs. Othon Redionitis and Eric Petersen. Also, Ian Neel for his work and help with the turning vane design.

TABLE OF CONTENTS

Page

LIST OF FIGURES

LIST OF TABLES

CHAPTER I

MOTIVATION AND INTRODUCTION

The Oran W. Nicks Low-Speed Wind Tunnel (LSWT) at Texas A&M University was built in the mid 1940's as an open circuit wind tunnel, shown in Fig 1. In 1958, construction began to close the circuit. A picture taken during this construction is given in Fig. 2. At this time, the main external balance was added to to structure. As a closed circuit wind tunnel, the LSWT has tested a wide range of articles. These include many fixed wing and rotary aircraft, rockets, parachutes, the Apollo capsule, the Space Shuttle, race car wings, motorcycles, bicyclists, oil drilling platforms and ships, electric wind generators, and a number of other articles. The layout of the LSWT facility can be seen in Fig. 3

The LSWT is to be used to study dynamic stall of helicopter blades at Mach 0.4, and potentially, 0.5. Reaching this Mach number range can produce shocks at the pressure minimum during pitch up and lead to violent dynamic stall [3]. Test Mach numbers exceed the current operating limit of the LSWT 7 x 10 foot test section which is approximately M=0.26, due to the load limits on the existing structure. A narrower test section would allow the model to be designed to withstand anticipated loads. The new construction would also be designed to withstand the increased static pressure loads. The test section dimensions will be 5 x 6 feet.

Early analysis with this reduction in area, and power results from the original motor, showed that the goal of reaching 0.5 Mach was only marginally achievable in

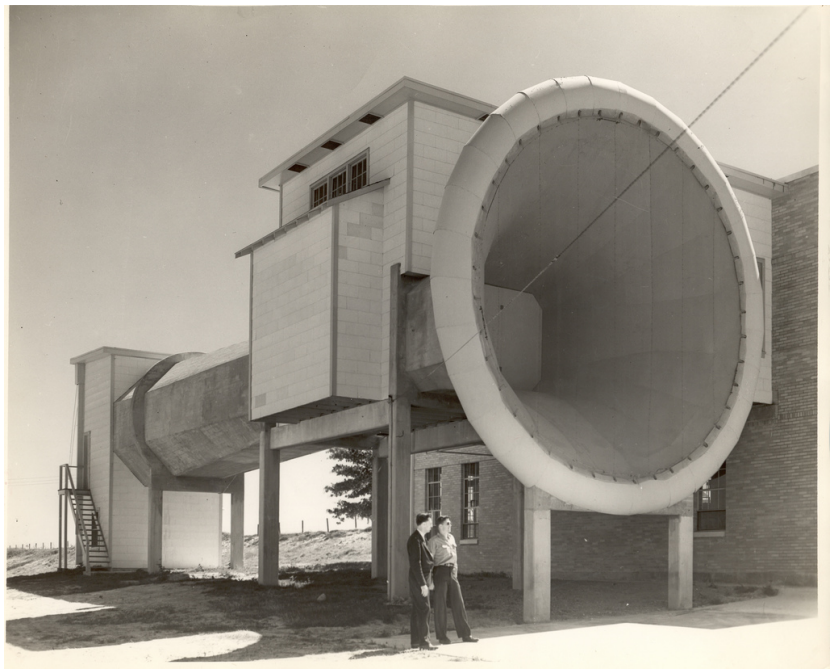

Fig. 1: Original open circuit design of the LSWT [1].

Fig. 2: Construction of the LSWT tunnel shell in 1958 to close the circuit [2].

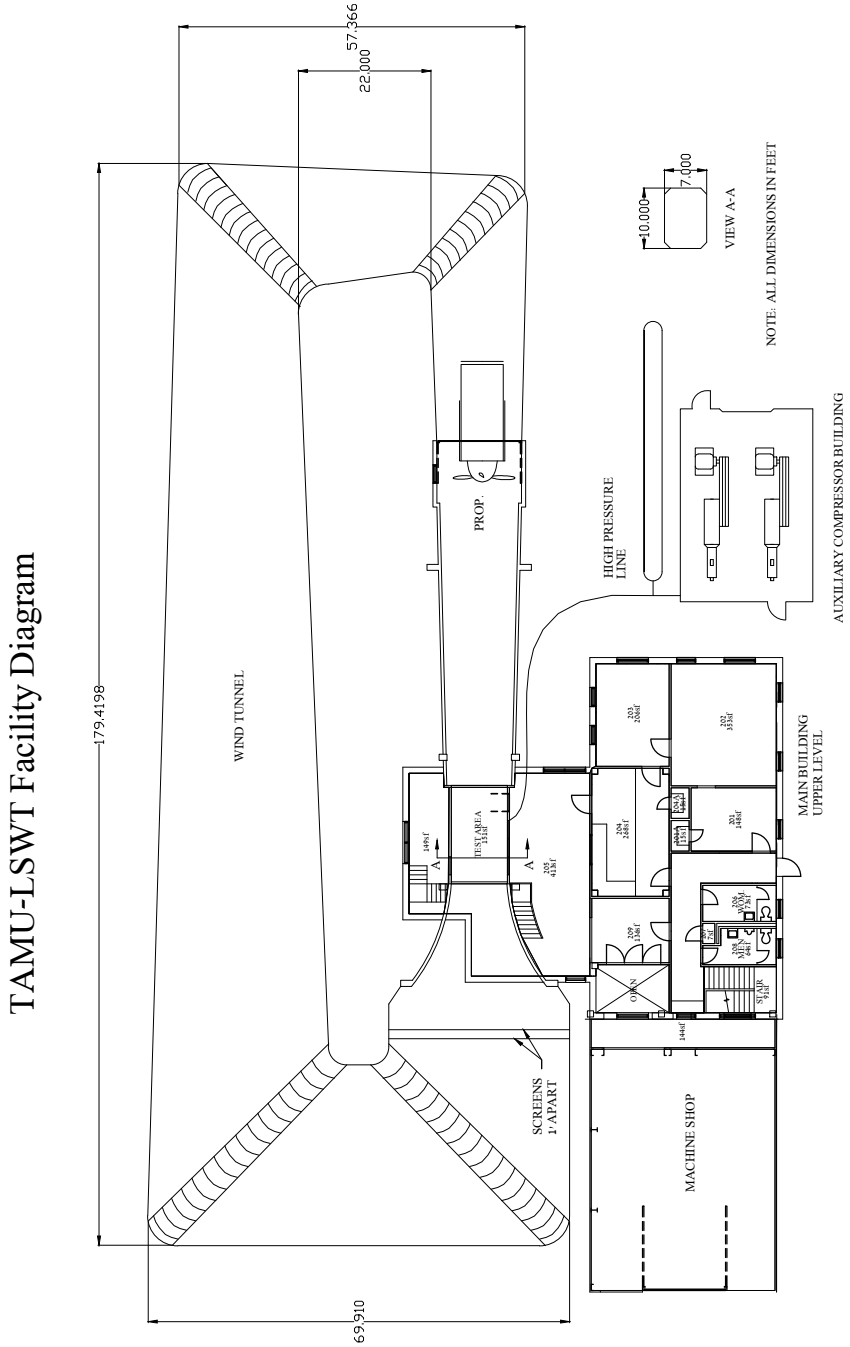

Fig. 3: Layout of LSWT circuit and connected facilities.

an empty test section. As a result, to improve the likelihood of success, a detailed study of the flow in the circuit was conducted. The losses in each section of the tunnel circuit were examined to determine what improvements might make the most impact to the overall efficiency of the tunnel. Further estimations, using power data from the new motor and loss estimations for the circuit, showed that with a well designed test section, contraction, and diffuser inserts, this goal is achievable with no further modifications to the remainder of the wind tunnel circuit.

The current state of the flow through the circuit of the LSWT will be presented in Chapter II. This includes results from theoretical analyses, tufting runs, and circuit pressure measurements. Chapter III will describe a study of the turning vanes of the wind tunnel and a method by which the power lost at this section can be decreased. The methodology for the design of the required diffuser changes for the reduced test section will be explained in Chapter IV. Chapter V will summarize the results from all three studies and will give recommendations for future action.

CHAPTER II

ASSESSMENT OF CURRENT FACILITY

As air moves through the circuit of the wind tunnel, there are losses related to the skin friction along the tunnel walls, losses related to changes in area or direction, and objects creating drag. If there were no losses through the circuit, the total pressure, static pressure, and dynamic pressure would all be related by Bernoulli's equation. Given the geometry of the LSWT circuit, this would look like the plot in Fig. 4. As a consequence, once the air has been started it would continue circulating through the tunnel. Since there are losses in the circuit, when the tunnel is running at a steady state the motor is working to only overcome these losses. If these losses can be minimized, the power required to run the tunnel will decrease, resulting in a savings of many thousands of dollars per year.

II A. LSWT Features and Operating Strategy

The LSWT has a circuit length of 400 ft. This long length allows for the cross sectional area to expand from a test section area of 68 ft^2 to a maximum of 707 ft^2. As the area expands, the velocity decreases proportionally. The power losses due to drag are proportional to the cube of the velocity. However, if the area is expanded too rapidly, there is risk of the flow becoming separated and causing increased power loss and unfavorable test conditions. The long length of the tunnel also allows turbulence created at the fan to dissipate.

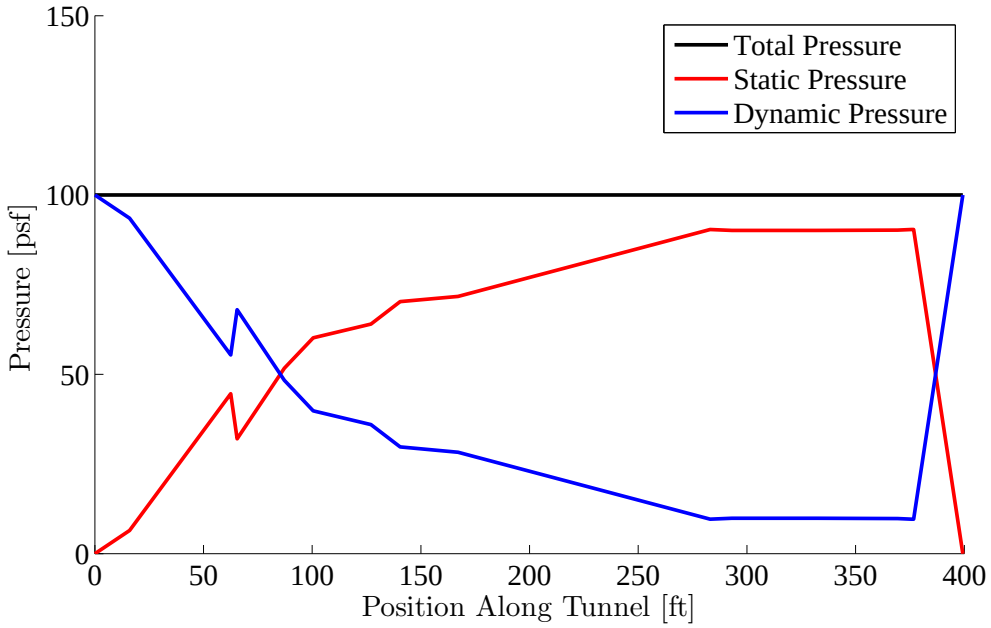

Fig. 4: For an ideal wind tunnel circuit there are no pressure losses. The total pressure remains constant and the static and dynamic pressure are proportional to the area.

Starting at the end of the test section, the primary diffuser begins to expand the cross sectional area. A view looking from the test section down the diffuser can be seen in Fig. 5. A conventional wind tunnel would then consist of two 90° corners and the power section. As a result of the LSWT originally being an open circuit configuration, the fan and motor are upwind of the first two turns, and split the primary diffuser into two sections. The advantages of the traditional design are that if a model fails during a test and becomes loose, there is a reduced risk of it hitting the fan blades and potentially destroying them. A second advantage is that if the fan is downwind of the entire primary diffuser the cross sectional area is larger. A larger, slower propeller will generally operate more efficiently than a smaller, faster

turning one. Turns one and two of the LSWT are largely constant area turns, with an area increase of only 18 ft^2 across turn one and an area decrease of 8 ft^2 across turn two.

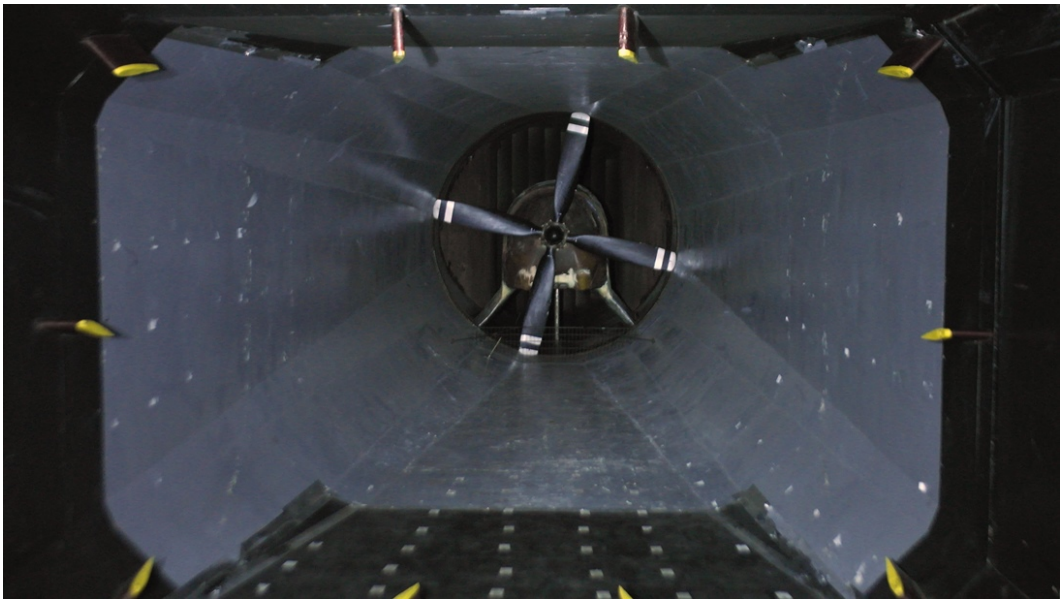

Fig. 5: The first section of the primary diffuser extends from the end of the test section to the fan. The vortex generators, seen along the walls at the exit of the test section help to keep the flow along the diffuser walls attached.

The secondary diffuser begins a few feet downwind of turn two and is circular. The 126 ft long diffuser expands from 240 ft^2 to 706 ft^2. There is a thermal expansion joint in the middle of the secondary diffuser which allows the steel shell to expand or contract with changing temperatures. Turns three and four are 30 ft in diameter and turn the flow back around 180°. Turn three can be seen in Fig. 6 during its installation in 1958. There are a set of two mesh screens downwind of turn four. This is an optimal location for the screens since the local velocity is the slowest of

the entire circuit, resulting in smaller pressure and power losses. The screens help to clean up the flow by distributing any unevenness. The contraction section then draws the flow from the settling chamber to the test section with a contraction ratio of 10.4:1. The contraction can be seen in Fig. 2.

Fig. 6: The 30 ft diameter turning vane section of turn three can be seen here during the construction of the tunnel shell in 1958 [4].

For a test at the LSWT, a target dynamic pressure, or 'q', is most commonly used to drive the velocity of the flow in the test section. The velocity to dynamic pressure relation is given in Eq. 2.1, where ρ is the local static density. Closed circuit

wind tunnels vent at a location to allow the circuit to breathe during startup and shut down. The LSWT vent location is at the test section. This makes the static pressure at the test section closest to atmospheric pressure, therefore putting the lowest stresses on the walls at this location. There are also leaks throughout the circuit of the LSWT. The vent section acts to make up for this lost air.

$$q = {}^{1}\!/_{2}\rho V^2 \tag{2.1}$$

The leaks in the tunnel are a source of pressure loss throughout the circuit. However, the main source of pressure and power loss are due to friction on the tunnel walls. Since the skin friction drag is proportional to the velocity squared, it is helpful to have the flow as slow as possible for everywhere but the test section. This is done through the two diffuser sections of the tunnel. The first diffuser section increases the area from 68 square feet at the test section to 269 square feet between turns one and two. The second diffuser extends from turn two to turn three and increases the area to 707 square feet over a length of 116 feet.

Three types of flow exist in the LSWT circuit, laminar, turbulent, and separated. Laminar flow is the most favorable for good flow quality testing and low frictional power losses. Turbulence is usually unfavorable for testing and is deleterious to the energy of the flow throughout the circuit. However, a turbulent boundary layer is preferred if the alternative is separation around corners and diffusers. This can sometimes be the case since a turbulent boundary layer helps to keep flow attached. Separated flow causes the largest preventable power losses in a tunnel circuit. If an adverse pressure gradient along a surface is too great for the flow's momentum

to overcome, separation will occur. There are additional concerns to consider with separation as well. If the separation is unsteady, the oscillations will lead to vibrations in the structure, surging in the test section, and oscillatory loads on the fan.

It is possible to estimate where separation is likely to occur in a flow. It is also possible to observe. Areas of special interest within the circuit were qualitatively measured using a series of tuft runs.

II B. Theoretical Analysis of Circuit

NASA Technical Note D-8243 [5] outlines a methodology for estimating the losses in wind tunnels. The method used to specifically analyze the LSWT will be summarized here. Firstly the circuit is broken into a series of sections. These sections consist of constant area ducts, open-throat ducts, contractions, constant area and diffusing corners, diffusers, exit, fan section, flow straighteners, internal flow obstructions, perforated plates, mesh screens, sudden expansions, and vaned diffusers. The LSWT circuit only consists of constant area ducts, contractions, corners, a power section, mesh screens, and diffusers. The loss coefficient determined for each section is given by

$$K = \frac{\Delta H_l}{q_l} \tag{2.2}$$

where ΔH_l is the local drop in total pressure along a section, and q_l is the dynamic pressure at the inlet of a section. The loss coefficient is useful for relating the pressure losses for a given section at different testing speeds.

For each section, the local Mach number must be known. To determine this,

the equation

$$MA\left\{\frac{\gamma+1}{2\left[1+\left(\frac{\gamma-1}{2}M^2\right)\right]}\right\}^{\frac{\gamma+1}{2(\gamma-1)}} = constant \tag{2.3}$$

is used. For Mach numbers below 0.3 the incompressible continuity equation is a good approximation of this relation. However, since the losses will be estimated up to a test section Mach number of 0.5, Eqn. 2.3 will be used. The constant is calculated from the conditions at the test section.

For a given estimation, the test section Mach number and cross sectional area is given. The static pressure and temperature are assumed for average running conditions as 1 atmosphere and 80°F. The static density at the test section is calculated from the ideal gas law, given by

$$p = \rho R_{spec} T \tag{2.4}$$

where R_{spec} is the specific gas constant of dry air.

The total temperature and density at the test section are then calculated using the isentropic flow relations:

$$T_0 = T\left(1+\frac{\gamma-1}{2}M^2\right) \tag{2.5}$$

$$\rho_0 = \rho\left(1+\frac{\gamma-1}{2}M^2\right)^{\frac{1}{\gamma-1}} \tag{2.6}$$

where T and ρ are the test section static temperature and density, respectively.

The speed of sound for the flow calculated at total, or stagnation, conditions is determined for an ideal gas with

$$a_0 = \sqrt{\gamma R_{spec} T_0} \tag{2.7}$$

where γ is equal to 1.4 for conditions seen at the LSWT. The speed of sound at static conditions is given by

$$a = a_0 \left(1 + \frac{\gamma - 1}{2} M^2\right)^{-1/2} \tag{2.8}$$

The total pressure is equated from Eq. 2.4 and the viscosity calculated at total conditions is calculated from Sutherland's Law, given as

$$\mu_0 = \mu_{ref} \left(\frac{T_{ref} + C}{T_0 + C}\right) \left(\frac{T_0}{T_{ref}}\right)^{3/2} \tag{2.9}$$

where $\mu_{ref} = 3.74 \times 10^{-7}\ lb_f s/ft^2$, $T_{ref} = 518.6\ R$, $C = 198.6\ R$ which are the reference viscosity, temperature, and constant for air, respectively, for Sutherland's Law [6]. The velocity at the test section, V_{ts} can then be calculated from

$$V = \frac{M}{a} \tag{2.10}$$

The Mach number at each section is determined with Eq. 2.3, where the constant is acquired by evaluating the equation with the test section Mach and area.

The Reynolds Number (Re) is needed for many of the sections and is determined from

$$Re = \frac{\rho_{ts} V_{ts} l_{ch}}{\mu_0} \left(\frac{A_{ts}}{A}\right) \left[1 + \left(\frac{\gamma - 1}{2} M^2\right)\right]^{0.76} \tag{2.11}$$

where ρ_{ts}, V_{ts}, A_{ts} are the test section static pressure, velocity, and area, respectively, A is the local area, and l_{ch} is the local characteristic length, usually the hydraulic diameter. The equation for hydraulic diameter used for this study is determined from

$$D_h = \frac{4A}{P} \tag{2.12}$$

where P is the wetted perimeter of the cross section.

Another value which must be obtained for each section is the friction factor. The friction factor can be obtained from the *Prandtl universal law of friction* [5], which has been simplified for a pipe with a roughness factor of zero. This is a suitable approximation for the large diameter versus roughness of the tunnel walls. The simplified friction law is given in Eq. 2.13, which relates the Reynolds number and friction factor for turbulent, fully developed pipe flow. The Re is the average for the section and as a result, both the inlet and exit hydraulic diameters and areas are needed for each section.

$$\frac{1}{\sqrt{f}} = 2\ \log_{10}\left(Re_{D_{h1}}\sqrt{f}\right) - 0.8 \tag{2.13}$$

With these values in hand, the loss coefficient for each section can be calculated.

Constant Area Duct: For a constant area duct, the loss coefficient is due to the wall friction, and is calculated from

$$K = \frac{fl}{D_h} \tag{2.14}$$

where l is the length of the section.

Contraction: In a contraction, the losses are mainly due to friction on the walls. The loss coefficient is approximated with

$$K = 0.32\frac{fl}{D_h} \tag{2.15}$$

Corners: The losses in a corner are composed of friction losses and rotational losses. For a corner where the area does not change from inlet to outlet, the loss

coefficient is approximated as

$$K = \frac{K_{TV}}{3}\left[2 + \left(\frac{log_{10}Re_{ref}}{log_{10}Re}\right)^{2.58}\right] \tag{2.16}$$

For a 90°corner, K_{TV} is approximately 0.15. The coefficients for other turning angles are given in Appendix B of NASA TN D-8243. The reference Re is 500,000. The characteristic length used for calculating the Re is the chord length of a turning vane. The corner length is measured along the center of the tunnel for the entire corner section.

This approximation is for a standard set of turning vanes where the gap to chord ratio is in the range of 2:1 and 4:1. The turning vanes at the LSWT have a chord length of 4.5 ft and gap of 2 ft, giving a ratio of 2.25:1. This equation does not take into account the shape of the turning vane. There are three commonly used shapes; a quarter circle, a quarter of a circle with an extension off the trailing edge, and a highly cambered airfoil. Barlow et al. give loss coefficients for early experiments with these three shapes as 0.200, 0.138, and 0.110 respectively [6]. More recent studies have given lower loss coefficients with the cambered airfoil design. Sahlin and Johansson [7] report a loss coefficient as low as 0.036. Their design is the basis for the experiment given in this paper in Chapter IV.

Fan (Power) Section: The power section should be treated as a series of contractions and diffusers.

Mesh Screen: The loss coefficient for a mesh screen is composed of coefficients that take into account the type of wire material, the Re of the flow, and the blockage

of the wire.

$$K = K_{Re} K_{mesh} \left(1 - \frac{A_{flow}}{A}\right) + \left(\frac{A}{A_{flow} - 1}\right)^2 \tag{2.17}$$

The Re for the screen section is determined from

$$Re = \frac{\rho V D_{mesh}}{\mu} \tag{2.18}$$

where D_{mesh} is the diameter of the wire used in the mesh. The wire diameter of the screen at the LSWT is 0.01 in and the wire mesh is 16 per inch, giving an A_{flow} value of $0.711A$.

The K_{Re} term in Eq. 2.17 is a function of the Re number for the screen section. For Re less than 400, the value is calculated as

$$K_{Re} = \frac{78.5\left(1 - \frac{Re}{354}\right)}{100} + 1.01 \tag{2.19}$$

For Re larger than 400, the value can be approximated as 1.

K_{mesh} is 1.3 for older, round, metal wire, 1.0 for new wire, and 2.1 for silk thread. A value of 1.3 was used for the following estimations.

Diffuser: The loss coefficient for a diffuser is made from the sum of the losses due to friction and due to expansion.

$$K = K_{expansion} + K_{fric} \tag{2.20}$$

The diffuser loss coefficient due to expansion, $K_{expansion}$ is given as

$$K_{expansion} = K_{exp} \left(\frac{AR - 1}{AR}\right)^2 \tag{2.21}$$

where K_{exp} is the net expansion loss determined for a given geometry as

$$K_{exp,circle} = \left\{ \begin{array}{ll} 0.1033 - 0.02389\theta & \text{for } 0 < \theta < 1.5^\circ \\ 0.1709 - 0.1170\theta + 0.03260\theta^2 + 0.001078\theta^3 & \\ -0.0009076\theta^4 - 0.00001331\theta^5 + 0.00001345\theta^6 & \text{for } 1.5^\circ \leq \theta \leq 5^\circ \end{array} \right\} \tag{2.22}$$

$$K_{exp,square} = \left\{ \begin{array}{ll} 0.09623 - 0.004152\theta & \text{for } 0 < \theta < 1.5^\circ \\ 0.1222 - 0.04590\theta + 0.02203\theta^2 - 0.003269\theta^3 & \\ -0.0006145\theta^4 + 0.00002800\theta^5 - 0.00002337\theta^6 & \text{for } 1.5^\circ \leq \theta \leq 5^\circ \end{array} \right\} \tag{2.23}$$

the equivalent conical angle, θ_{eq} is

$$\theta_{eq} = \tan^{-1}\left(\frac{1}{2}\frac{D_{h2} - D_{h1}}{L}\right) \tag{2.24}$$

where, D_{h1} and D_{h2} are the hydraulic diameters of the entrance and exit of the diffuser section, respectively, and the area ratio, AR is

$$AR = A_2/A_1 \tag{2.25}$$

The K_{fric} term for a conical expansion is given in Eq. 2.26, where f is the friction factor, obtained from Eq. 2.13.

$$K_{fric} = \frac{f}{8sin\theta_{eq}}\left(\frac{AR - 1}{AR}\right)^2 \tag{2.26}$$

The K_{exp} is found from experimental testing and is given for both circular and square cross sections in Eqs. 2.22 and 2.23 [5]. Each equation is piecewise for a range of equivalent cone angles.

Losses in the LSWT circuit were modeled using the method and equations given above. Once the loss coefficient is known for each section, an estimation of the power loss across that section can be calculated using Eq. 2.27 where A is the cross sectional area of the start of the section and V is the velocity of the flow at the start of the section. A map of the circuit with its different sections broken down is given in Fig. 7. The relevant dimensional properties for the start of each section is given in Table 1.

$$P_{loss} = \Delta H_l A V \tag{2.27}$$

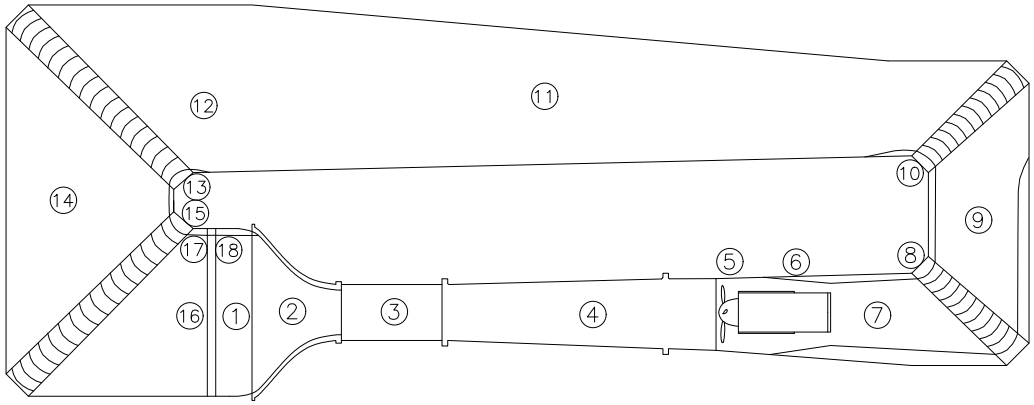

Fig. 7: Planview of wind tunnel circuit with locations of each section used in the theoretical model marked.

The corresponding estimated loss coefficients and power losses for each section are shown in Table 2. The losses were calculated at test section dynamic pressures of 50 and 100 psf, a static temperature of 80°F, and static pressure of 1 atm. These will be compared to actual measurements in the following section. According to this model the fan must provide 138 hp to the flow to maintain a dynamic pressure of 50 psf at the test section and 372 hp to maintain 100 psf.

Table 1: Values of LSWT sections for theoretical model, numbers match up with locations in Fig. 7

Number	Type	Length [ft]	Area [ft^2]	D_h [ft	θ_{eq} [deg]	AR	l_{ch} [ft]
1	Constant Area Duct	1.0	706.9	30.0	–	–	30.0
2	Contraction	22.6	706.9	30.0	25.69	10.4	30.0
3	Test Section (Diffuser)	16.0	68.0	8.6	0.39	1.1	8.6
4	Diffuser	46.5	72.7	8.4	2.54	1.7	8.4
5	Power Section (Contraction)	3.0	122.7	12.5	21.09	0.8	12.5
6	Power Section (Diffuser)	21.7	100.0	10.2	2.91	1.4	10.2
7	Diffuser	13.3	140.7	12.4	2.49	1.2	12.4
8	Corner 1	26.6	170.8	13.6	1.17	1.1	4.4
9	Diffuser	13.4	189.0	14.6	3.80	1.2	14.6
10	Corner 2	26.6	228.7	16.9	–	–	4.4
11	Diffuser	116.0	240.5	17.5	3.08	2.9	17.5
12	Contraction	10.0	706.9	30.0	2.14	1.0	30.0
13	Corner 3	37.1	689.2	29.3	–	–	5.0
14	Constant Area Duct	2.1	689.2	29.3	–	–	29.3
15	Corner 4	37.1	689.2	29.3	–	–	5.0
16	Constant Area Duct	6.4	695.6	29.5	–	–	29.5
17	Screen	–	706.9	30.0	–	–	30.0
18	Screen	–	706.9	30.0	–	–	30.0

Table 2: Estimated loss coefficients and power losses of the LSWT at various test section dynamic pressures for an 80°F test section.

		q=50 [psf]			q=100 [psf]		
Number	Type	Mach	K	P [hp]	Mach	K	P [hp]
1	Constant Area Duct	0.02	0.00	0.0	0.02	0.00	0.0
2	Contraction	0.02	0.01	0.1	0.02	0.01	0.2
3	Test Section (Diffuser)	0.18	0.02	25.1	0.26	0.02	67.3
4	Diffuser	0.17	0.03	33.8	0.24	0.03	91.8
5	Power Section (Contraction)	0.10	0.00	0.3	0.14	0.00	0.8
6	Power Section (Diffuser)	0.12	0.02	10.6	0.17	0.02	28.6
7	Diffuser	0.09	0.01	3.2	0.12	0.01	8.4
8	Corner 1	0.07	0.13	26.2	0.10	0.13	71.2
9	Diffuser	0.07	0.01	1.1	0.09	0.01	2.9
10	Corner 2	0.05	0.13	14.6	0.07	0.13	39.6
11	Diffuser	0.05	0.06	6.1	0.07	0.06	16.4
12	Contraction	0.02	0.00	0.0	0.02	0.00	0.0
13	Corner 3	0.02	0.14	1.7	0.03	0.13	4.4
14	Constant Area Duct	0.02	0.00	0.0	0.03	0.00	0.0
15	Corner 4	0.02	0.14	1.7	0.03	0.13	4.4
16	Constant Area Duct	0.02	0.00	0.0	0.02	0.00	0.1
17	Screen	0.02	0.57	6.6	0.02	0.57	18.1
18	Screen	0.02	0.57	6.6	0.02	0.57	18.1
	Total			137.6			372.3

II C. Circuit Performance Measurements

Two methods were used to assess the flow conditions through the wind tunnel circuit, tufting and pressure measurements. While there were a few places where separation was expected to be most likely in the circuit, a large area of the circuit was fitted with tufts. The pressure measurements were taken at the transition points of the different tunnel sections. Some of the sections were combined to decrease the number of needed pressure transducers.

II C. 1. Tuft Testing

Examining the inside of the wind tunnel circuit, there were multiple locations where separation seemed likely. The first is the back of the motor housing. Even though the expansion angle for this section is 2.91°, the housing meets at an angle of 40° and, intuitively, one would think that these large, abrupt changes in geometry would encourage separation. A downwind view of the housing can be seen in Fig. 8. Separation was also expected at an area where wooden inserts transition to the steel tunnel shell, shown in Fig. 9. This area also had a large expansion angle. A third location of expected separation was the turning vanes.

A series of tufting runs were conducted to determine which areas of interest showed signs of separation. Yarn, cut to 2 inch lengths, was taped or stapled to the tunnel walls, motor housing, and turning vanes. Cameras were set up to record the behavior of the tufts with the tunnel set at various dynamic pressures up to 50 psf in the test section. Ultraviolet lights were used to illuminate the fluorescent tufts without illuminating the tunnel to aid with visualization of the tufts in the video.

Fig. 8: View of downwind side of motor housing, showing the large diffuser angle off of the housing and the wood inserts on the tunnel walls.

Fig. 9: View of the wood insert between turns one and two. Separation was expected here due to the relatively abrupt area change along the last 5 feet of the insert.

The tuft runs revealed that the flow along the motor housing remained attached, but was very turbulent, as would be expected since it is downwind of the fan. This did not seem likely due to the large changes in geometry, however, further studying the geometry revealed why this was the case. When the tunnel shell was constructed, wood insert were installed to more slowly transition the cross sectional area off the downwind side of the motor housing. As-built drawings of the complex geometry of the power section were found. The cross sectional areas given in the drawings reveal that the power section has an area ratio of 1.41 and an equivalent conical expansion angle of 2.91°. These are within the recommendations for a diffuser and their significance will be expanded upon in Chapter IV. The reason that the diffusion properties are so well behaved, in spite of the motor housing creating a large amount of blockage, is that the wood inserts along the tunnel walls modify the geometry of the steel shell. These inserts begin near the middle of the power section, and continue to a few feet downstream of the second turn. The wood inserts at the power section can be seen in Fig. 8.

The next area where separation seemed likely to occur is at the transition from wood insert to metal tunnel shell located on the outer side of the circuit, between turns one and two. A picture looking from inside the tunnel at this location can be seen in Fig. 9. Separation is likely at this location since there is a relatively large change in the angle of the insert. The tuft runs revealed that there is a very small separation bubble at this location.

Although this study did not set out with the idea that separation at the turning vanes would be a main focus, tufting runs revealed that separation occurred imme-

diately off the leading edges on turns one and two. The separation along the upper side of the vanes was so violent that the tufts were shredded as shown in Fig. 10. A planview of the wind tunnel with the locations where separation was most expected and where it was actually found is shown in Fig. 11

The tufting runs show that separation is most prevalent on the first and second turning vane cascades, but not at turns three and four. This leads to the conclusion that improvements to the circuit efficiency will be most impactful by fixing these locations. Not only is separation most prevalent here, the velocity is high so the impact on power is high as well.

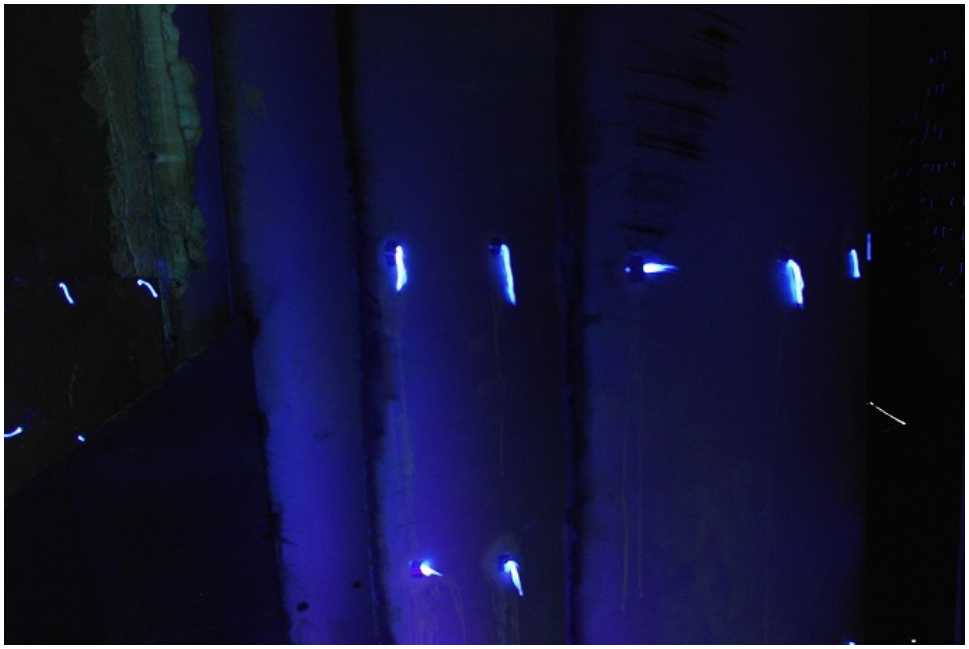

Fig. 10: Tufts on suction side of turning vane shredded due to separation.

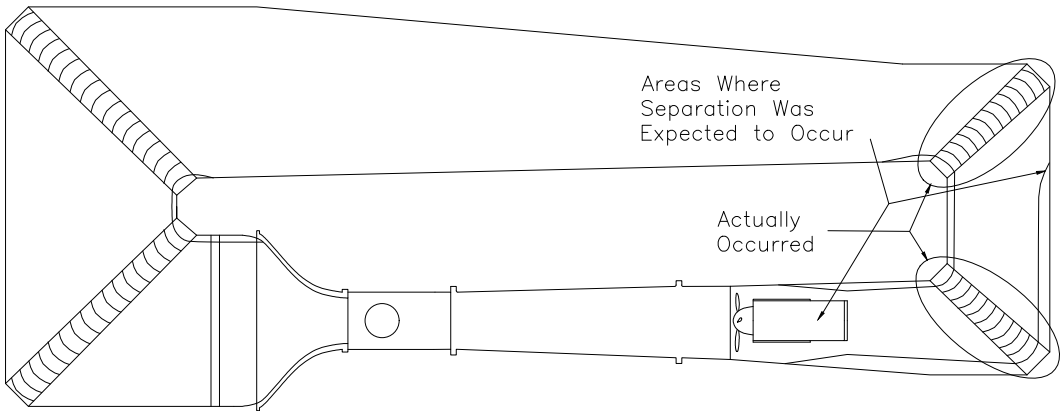

Fig. 11: Planview of wind tunnel circuit with locations of areas of expected separation noted.

II C. 2. Circuit Pressure Measuremtents

The different sections of the wind tunnel circuit were measured using seven Omega PX481A pressure transducers and the existing test section pitot-static probe and pressure transducers. The eight measured sections consisted of the test section plus first diffuser, power section, turn one, turn two, second diffuser, turns three and four, screens, and contraction. The locations where the pressure measurements were taken can be seen in Fig. 12.

Conduit was run along the circuit to house the cables for the transducers, an example of this can be seen in Fig. 13. The locations of the pressure taps in the tunnel were made along the inner side of the circuit, this minimized the amount of cable and conduit needed. For the static measurements, the tunnel wall was drilled and tapped with 1/8 NPT thread, which matched the thread of the transducer. The transducer was screwed into the hole, ensuring that the tip of the transducer did

not protrude into the flow. For total pressure measurements, a set of pitot tubes were made from 0.25 in bent brass tubing, with adapters at the base. To keep the measurement outside of the boundary layer of the tunnel, the pitot tubes stood out 12 in from the wall. A pitot tube placed behind the power section can be seen in Fig. 14. To change from a static measurement to a total pressure measurement, the transducer is removed from the tunnel wall, the pitot tube is screwed in in its place, then the transducer is screwed into the adapter of the pitot tube. While this method did not allow for measurement of both the static and total pressure along the circuit at the same time, it halved the number of required transducers.

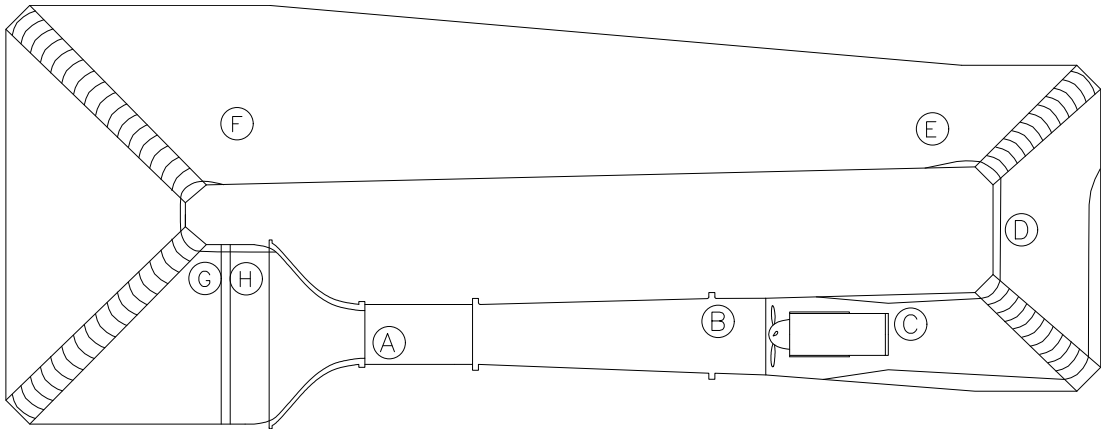

Fig. 12: Planview of wind tunnel circuit with locations of pressure taps marked.

A set of runs were made to measure the static and total pressure throughout the tunnel. The first run was made with the fan speed set to 900 RPM and the second run was with the fan at 1200 RPM. These two configurations were then repeated, taking total pressure measurements. Pressure coefficients for these runs

Fig. 13: Conduit along wind tunnel for wiring of circuit pressure transducers.

Fig. 14: Pitot tube inside tunnel, behind power section.

were calculated using Eqs. 2.28 and 2.29, where the subscript 'ts' stands for the test section value.

$$Cp_0 = \frac{p_0 - p_{0,ts}}{q_{ts}} \tag{2.28}$$

$$Cp = \frac{p - p_{ts}}{q_{ts}} \tag{2.29}$$

For the runs, the values below q=40 psf were removed since they were drastically off from the other values. This has been attributed to the fan creating large amounts of turbulence at such high speeds and low pitch values and also due to a smaller signal to noise ratio of the pressure transducers.

In Fig. 15, the values for total pressure seem reasonable for the range of q=50 psf up to q=100 psf, then back down to q=80 psf. From station A to B, it would be expected that there would be a large drop in total pressure across the test section and first diffuser since these areas have the highest speeds and as a result, the largest amount of skin friction. The lack of this in the data could indicate measurement of station B is too close to the fan. The pitot tube was installed 7 ft upstream of the fan plane. As would be expected, there is a large increase of total pressure across the fan (stations B to C in Fig. 12). Because measurements at station B are not believed to be correct, the increase in total pressure across the fan is not as large as it should be. Across turns one and two, stations C to E, there is a decrease in total pressure, with more of a decrease across turn one than turn two. This is a result of the flow moving slower across turn two after a slight expansion between the corners. The second diffuser is between stations E to F, most of the measurements show a slight decrease in total pressure, as would be expected. A few do show an increase, however. This is possibly due to the air, tunnel shell, tunnel cooling sytem,

and outside temperature not being at thermal equilibrium. The turbulence in the air and the friction with the walls all turn into heat, the shell heats up as it absorbs this energy. As the run progresses, the shell can not absorb heat at the rate it is being created. This is supported by the measurements taken at the end of the extended runs. As the speed is decreased near the end of a run, measurements tend to disagree more and more with the measurement taken earlier in the run. It would be worthwhile to repeat these measurements in the winter to determine how much of an effect the heat transfer with the walls causes this. Across the screens, stations G to H, there is a decrease in total pressure, then across the contraction section there is another slight decrease in total pressure.

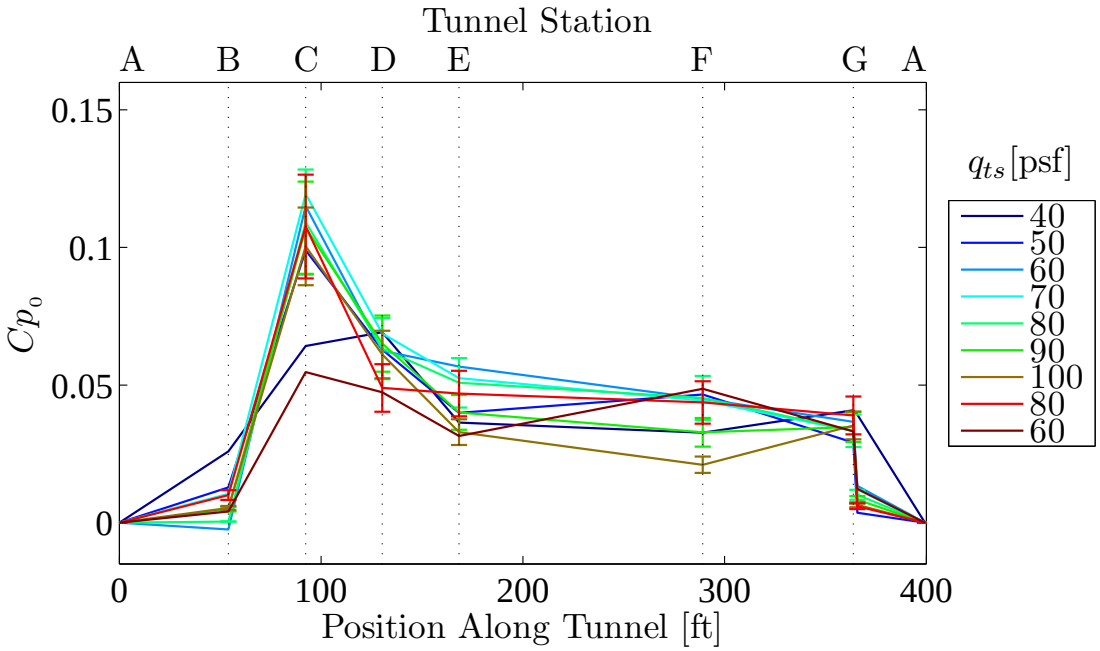

Fig. 15: Total Pressure Coefficient from run at 900 RPM. For tunnel stations, refer to Fig. 12.

The results from the static pressure measurements for the 900 RPM run are shown in Fig. 16. This plot shows that as the air moves from station A to station C, the entrance of the test section to upstream of corner one, the static pressure increases, this due to the expansion along these two sections. From station C to station D, corner one, there is a slight decrease in static pressure, even though the geometry is slightly expanding. This is likely caused by the separation at the leading edge of the turning vanes and resultant turbulence constricting the flow. Turn two shows an increase in total pressure, this points to the flow being better behaved across this turn, possibly in part as a result of the turning vane corrections which will be addressed in the following chapter. The second diffuser is from stations E to F. For this area, the static pressure should be decreasing. However, a number of the runs show an increase. This is likely a result of the temperature issue discussed for the total pressure at this location. There is then a very large static pressure drop across the contraction as the speed of the flow increases.

Comparisons with the theoretical model and measurements made from the 900 RPM run are given in Figs. 17 and 18. These plots show the significance in the measurement from the test section to the fan. The test section and primary diffuser, according to the theoretical model, should be an area of large pressure losses. The measurements do not corroborate this. Since this is the area where velocity is the highest, the losses due to friction on the walls will also be greatest. This measurement error means that a reliable circuit total of the total pressure losses can not be obtained from the data. If it is assumed that the largest errors in measurement occurred across this section due to bad placement of the transducer upstream of the fan, the data

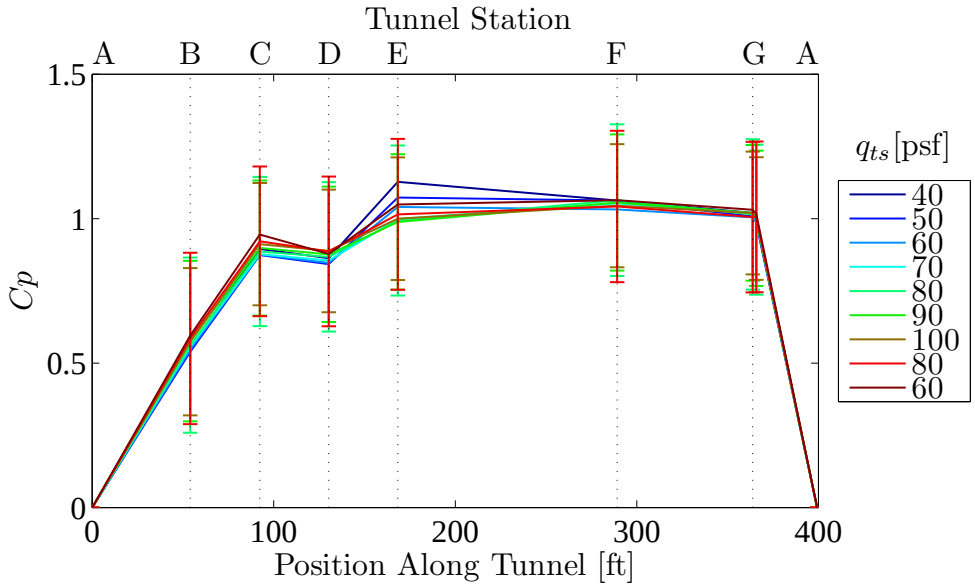

Fig. 16: Static Pressure Coefficient from run at 900 RPM. For tunnel stations, refer to Fig. 12.

still shows that the measured values across turns one and two are larger than the estimated loss. This would certainly be a result of the separation found in the tuft runs. The results from the comparison are also summarized in Table 3.

If it is again assumed that the total pressure losses measured downstream of the fan are correct, and the pressure loss for the test section and diffuser is replaced by the theoretical loss, an estimation of the fan/motor system efficiency can be calculated using :

$$\eta_f = \frac{P_{aero\ losses}}{P_{electrical\ input}} \tag{2.30}$$

where η_f is the efficiency of the entire motor and fan system, the aerodynamic power losses are calculated from the estimated total pressure increase across the fan, and the electrical power input is how much power is fed into the motor. For a test section

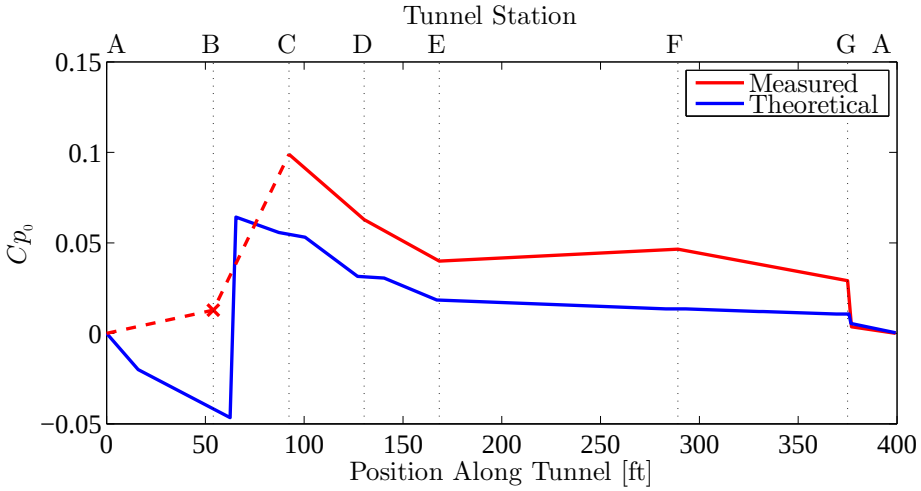

Fig. 17: Comparison of measured total pressure loss along circuit with theoretical losses at a test section dynamic pressure of 50 psf. Measurement at station B is unrepresentative of pressure losses in circuit, likely due to bad placement. For tunnel stations, refer to Fig. 12.

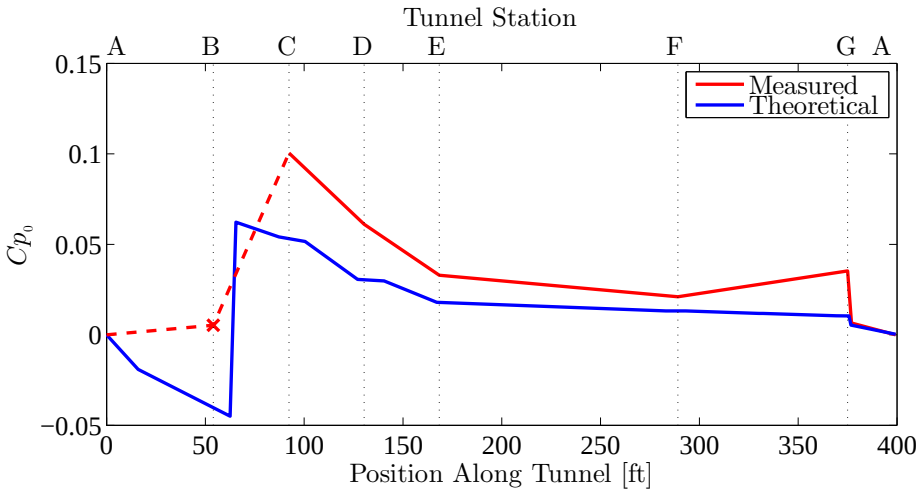

Fig. 18: Comparison of measured total pressure loss along circuit with theoretical losses at a test section dynamic pressure of 100 psf. Measurement at station B is unrepresentative of pressure losses in circuit, likely due to bad placement. For tunnel stations, refer to Fig. 12.

Table 3: Measured and Estimated total pressure losses [psf] for test section dynamic pressures of 50 psf and 100 psf.

	q=50 [psf]		q=100 [psf]	
Section	$\Delta p_{0,measured}$	$\Delta p_{0,estimated}$	$\Delta p_{0,measured}$	$\Delta p_{0,estimated}$
Test Section and Diffuser	-0.67	2.40	-0.53	4.59
Motor	–	0.52	–	0.98
Corner 1	1.89	1.22	4.10	2.25
Corner 2	1.20	0.66	2.94	1.20
Secondary Difffuser	-0.35	0.25	1.24	0.48
Corners 3 and 4	0.91	0.15	-1.49	0.26
Screens	1.34	0.54	3.01	1.06
Contraction	0.187	0.00	0.68	0.00
Total	4.51	5.75	9.91	10.84

dynamic pressure of 50 psf, the η_f is 61.5%. For q=75 psf the efficincy is 76.5% and it is 68% efficient for q=100 psf. Meaning that the peak efficiency for 900 RPM and an empty test section is somewhere between 50 and 100 psf.

The total pressure results for a 1200 RPM run, shown in Fig. 19 are not as clear as the 900 RPM results. Many of the test speeds show a decrease or little to no increase in the total pressure across the fan. Only at 70 psf and up does the total pressure across the fan increase. This could signify that at 1200 RPM, the flow is too turbulent at lower test section speeds for the measurement method used to get an accurate result. This is supported by comparing the power input to the motor for the 900 and 1200 RPM runs, presented in Fig. 20. For a motor setting of 1200 RPM the power draw is higher than that for the 900 RPM setting, the difference is greatest at lower test section dynamice pressures. At these slower speeds the motor is much more inefficient at the higher RPM setting. This extra power is being used

to create more turbulence in the flow.

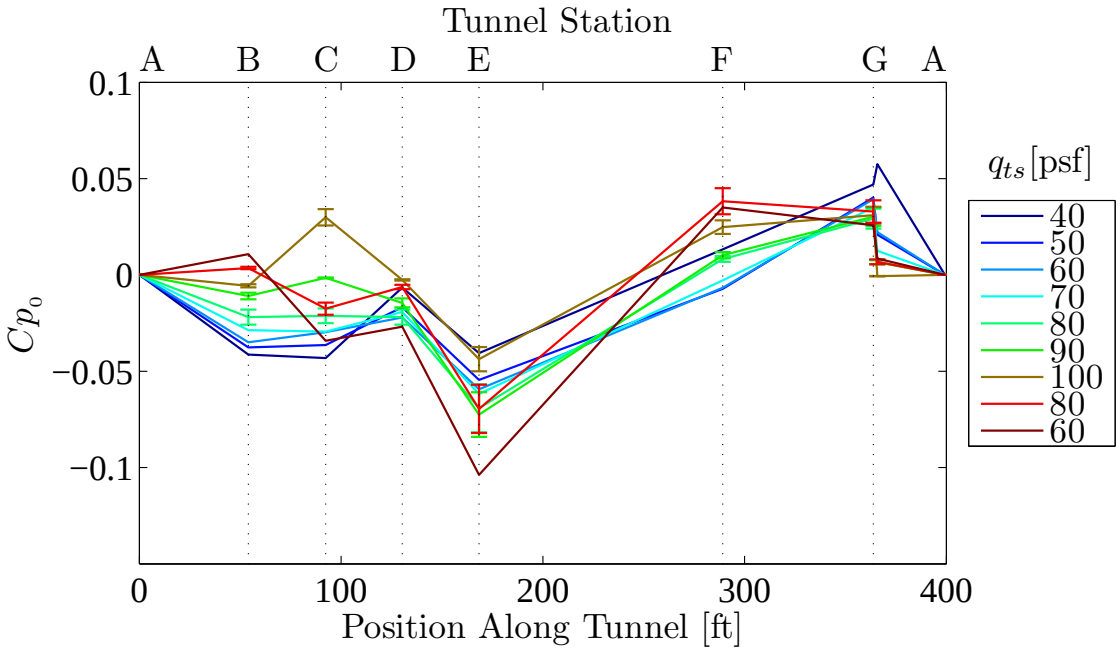

Fig. 19: Total Pressure Coefficient from run at 1200 RPM. For tunnel stations, refer to Fig. 12.

Fig. 21 gives the static pressures of the circuit for an RPM value of 1200. The static pressure increases from the test section to upwind of turn one as the area increases. It then drops slightly across turns one and two. This is likely due to the increased turbulence at this high RPM value. There is less of a pressure drop at the higher dynamic pressures as a result of the ever increasing efficiency of the fan. As the flow continues through the second diffuser the turbulence dies out and the area increases, increasing the static pressure. The static pressure then decreases across the contraction section.

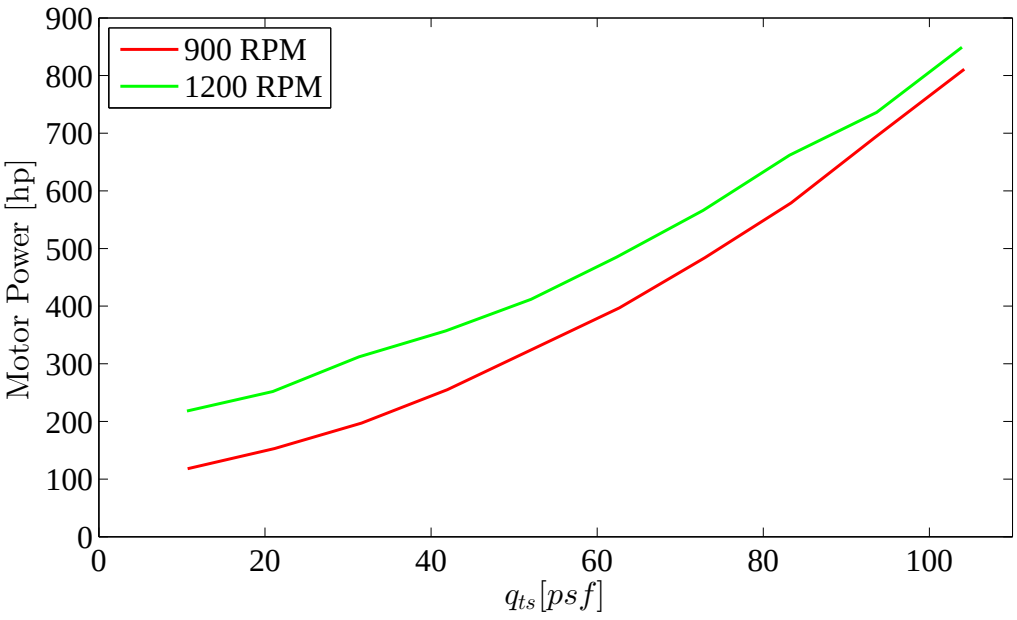

Fig. 20: Comparison of motor input vs. test section speed for motor RPM settngs of 900 and 1200

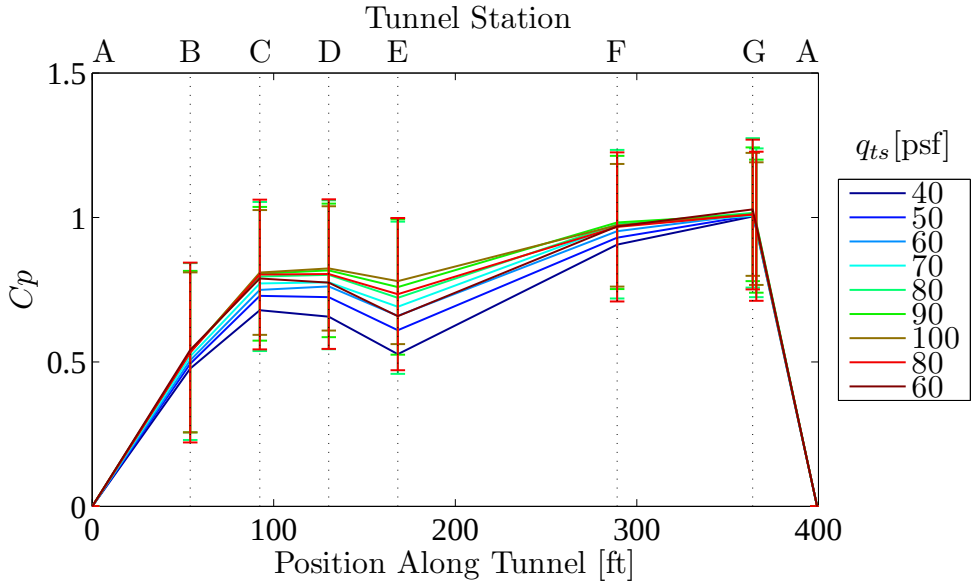

Fig. 21: Static Pressure Coefficient from run at 1200 RPM. For tunnel stations, refer to Fig. 12.

II C. 3. Recommendations

The power comparison revealed that for an empty test section, it is more efficient to run at 900 RPM then 1200 RPM. Therefore, the tunnel should generally be operated around this RPM, unless large drag in the test section requires a higher RPM setting. Extrapolating to higher speeds, 1200 RPM is expected to be more efficient only beyond q=125 psf in the test section.

Measuring the total pressure increase across the fan is essential to determining the efficiency of the power system. The existing pressure system could be iterated upon until believable results are obtained. A total and static pressure rake system could be designed to be put in place upstream and downstream of the motor. The upstream measurement should also be taken at different distances from the fan plane to determine where the effects from the fan become negligible.

To obtain better measurements for the remainder of the circuit locations, a static pressure ring system could be used to negate errors in measurement due to flow nonuniformity. This change would require no new instrumentation but substantially more labor.

The largest pressure losses were seen in turns one and two, and are assumed to also exist in the test section and first diffuser. These are the areas where decreasing the loss coefficient would be most useful. For the test section and diffuser, not much can be done besides increasing the smoothness of the walls. The losses at the turning vanes can be improved. If the flow can be kept from separating at the turning vanes, not only will the losses at the corners improve, but the the flow through the circuit will be cleaner, and potentially improve the flow quality in the test section. A method for doing this follows in the next chapter.

CHAPTER III

TURNING VANES

The existing turning vanes in the LSWT are bent 0.25 inch steel plate. They are designed as a quarter circle with a 28 inch extended straight trailing edge. The tufting runs revealed that separation occurs at the leading edge of the turning vanes on turns one and two, with little to no separation occurring at turns three and four, up to a measured dynamic pressure of 50 psf in the test section. A glove system was designed to retrofit the existing turning vanes. The geometry for the glove approximates the design by Sahlin and Johansson [7] with modifications to fit the existing structure. A proof of concept of the system was installed on three turning vanes at turn two. The system successfully maintains attached flow up to 100 psf at the test section. Before and after the installation of the turning vane gloves a traverse system was installed upstream, then moved to downstream of the section. The traverse took total and static pressure measurements to assess the flow. These measurements show an improvement to the power lost across the turning vanes.

III A. Current Vane Design and Power Loss

An automated traverse system was designed and fabricated to take total and static measurements upstream and downstream of the central turning vane of the second turn cascade. The traverse was set up so that the line of measurement was parallel to the cascade, while the pressure tube was parallel to the assumed flow.

The total traversed width was 30 in, 6 in wider than the gap length. Measurements were taken at intervals of 10 cm upstream of the cascade at test section dynamic pressures of 50, 75, and 100 psf. The traverse was then moved downstream of turn 2, with the central vane of the cascade centered on the traverse again. For test section dynamic pressures of 50 and 75 psf the measurement spacing was 5 cm, for 100 psf the spacing was 3 cm. The total pressure, static pressure, and dynamic pressure for the existing vanes can be seen in Figs. 22 to 24. The measurements were converted to coefficients using Eqs. 2.28, 2.29 and

$$Cq = \frac{q - q_{ts}}{q_{ts}} \tag{3.1}$$

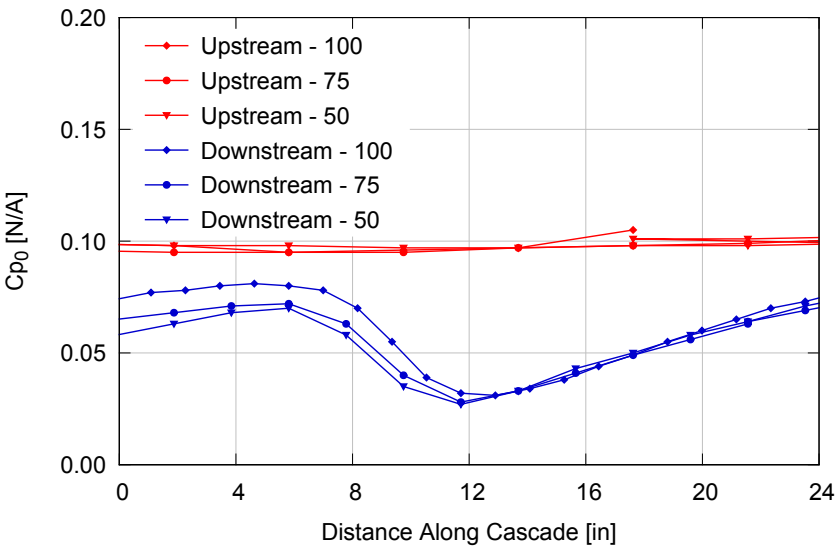

Fig. 22: Nondimensionalized total pressure upstream and downstream of existing turning vane cascade at turn two. Test section dynamic pressures of 100, 75, and 50 psf.

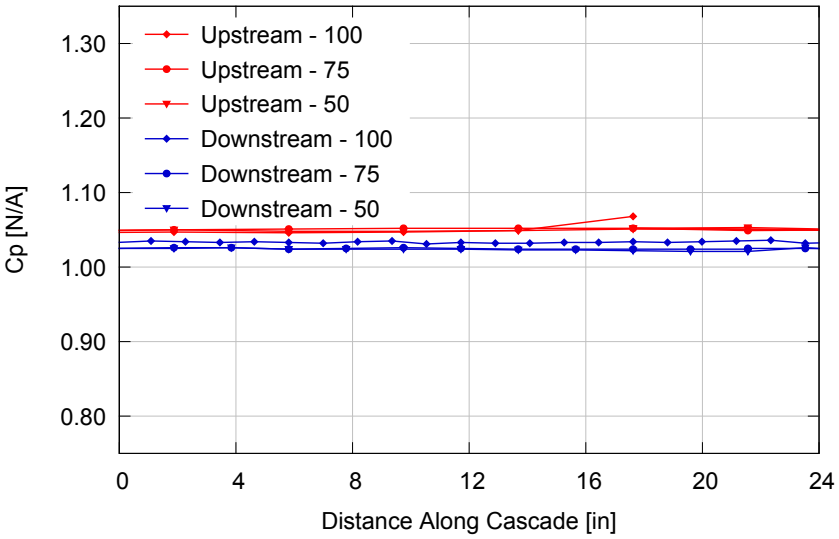

Fig. 23: Nondimensionalized static pressure upstream and downstream of existing turning vane cascade at turn two. Test section dynamic pressures of 100, 75, and 50 psf.

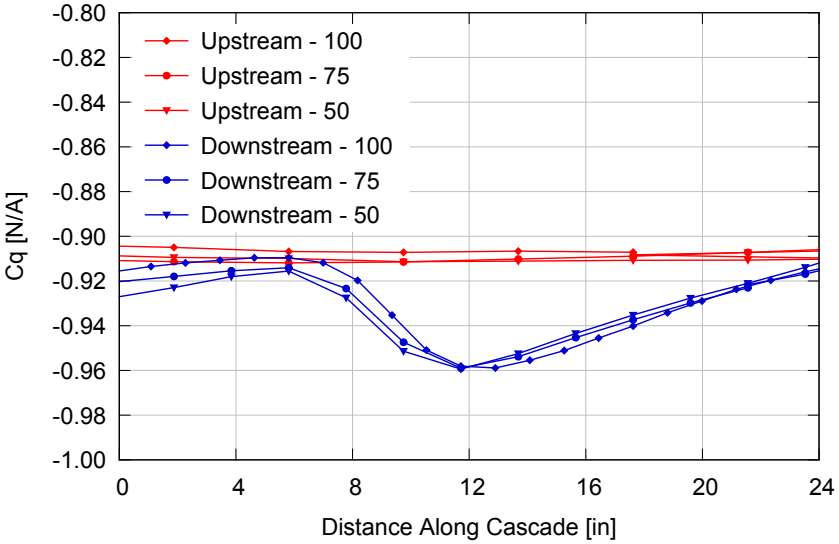

Fig. 24: Nondimensionalized dynamic pressure upstream and downstream of existing turning vane cascade at turn two. Test section dynamic pressures of 100, 75, and 50 psf.

The total calculated power loss and loss coefficient for all three of these runs are summarized in Table. 4.

Table 4: Power loss and loss coefficient for current vane shape at turn two.

Test Section q	Power [hp]	K
50q	57.0	0.475
75q	106.5	0.488
100q	148.2	0.415

The mass flow is proportional to the velocity, or the square root of the dynamic pressure. If the mass flow upstream of the vane is compared to the mass flow downstream of the vane, 14% of it is missing, as shown in Fig. 25. The error in measurement is most likely due to the traverse mechanism causing the flow in the turning vanes to be altered by causing increased separation on the vane and therefore more sensitive blockage.

Regardless of the precise loss values, it is clear that better performance is possible and should be pursued. If future measurements are carried out, changes to the traverse system could be made to give better results. The traverse stand should be shortened so that there is less blockage and resultant turbulence is minimized. The pitot tube holder should include a 2 to 3 ft vertical member to increase the distance between the flow being measured and the traverse.

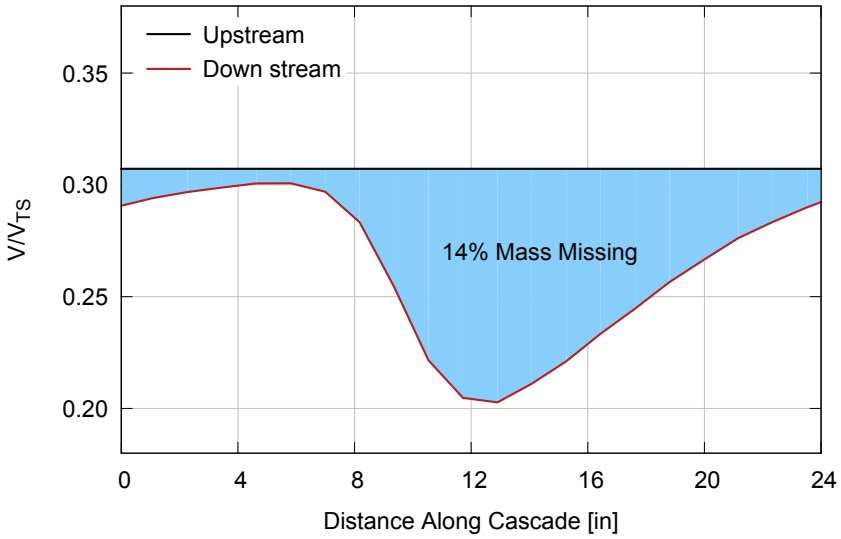

Fig. 25: Comparison of the upstream and downstream velocity of the central vane at turn 2 for q=100 psf in the test section, showing the mass loss in the measurement.

III B. Modified Vane Design

The lowest loss coefficient reported is found in Sahlin and Johansson's *Design of Guide Vanes for Minimizing the Pressure Loss in Sharp Bends* [7]. The design process starts by selecting an airfoil with a high lift to drag ratio for straight free stream conditions and good proven characteristics at low Reynolds numbers. The chosen airfoil is the Wortmann FX60-100. A potential flow program is used to design a 90° turning vane to replicate the pressure distribution along the low pressure side of the airfoil at its angle of attack with highest L/D. This design was tested by Sahlin and Johansson in a 0.3 x 0.28 meter duct wind tunnel. At Reynolds numbers above 100,000 this experiment gave loss coefficients of 0.04 or lower, with measurements taken up to Re=150,000. Comparatively, turns one and two of the LSWT operate

at Reynolds numbers of 2,750,000 and 2,250,000, respectively, at the current highest operating dynamic pressure of 100 psf in the test section.

The turning vane modifications were designed so that they meet the profile of the SA-070.61 as closely as possible while fitting over the existing turning vanes. A comparison of the SA-070.61 and the as-designed turning vane profiles can be seen in Fig. 26. The high pressure side of the modification is the existing turning vane, while the low pressure side matches the SA-070.61 profile. Two properties of this design will significantly improve the flow through the turns. First, the leading edge will have a radius of 0.56 in, the current vane leading edge is the rough, plasma cut edge of the 0.25 in steel plate. Second, the added thickness will improve the pressure gradient through the turn. A profile view of the existing turning vane with a representation of the modifications can be seen in Fig. 27.

The vane glove design consists of pressure treated wood ribs and bent 20-gage galvanized steel sheets. The ribs were designed as two sections so that they could be made from standard-sized lumber and to permit some adjustment as the ribs are bolted to the existing structure. Figs. 28 and 29 show a rib bolted to the existing structure. These photos also show the grooves designed into the wood ribs which give room for the heads of the mounting bolts. Three ribs are used to support each of the 3 ft tall skins, one each on the top and bottom, and one in the middle. The skins were shaped to meet the profile of the rib before installation. Three turning vanes on turn two were fit with the modification. They can be seen in Figs. 30 and 31.

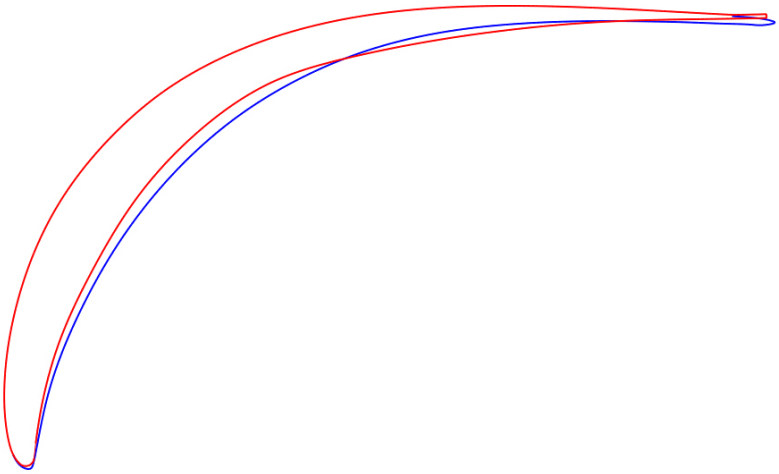

Fig. 26: Cross section of SA-070.61 compared to modified design used for turning vane glove. Blue is SA-070.61, red is design used for LSWT turning vane modifications.

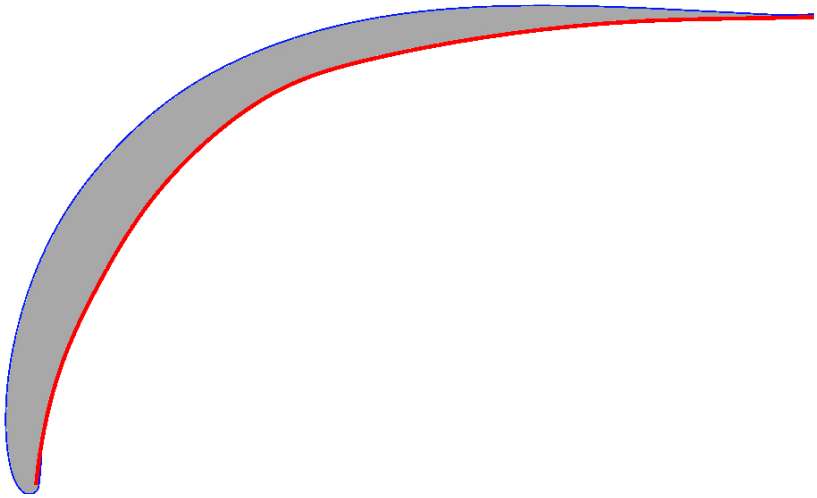

Fig. 27: Cross section of modified turning vane design. Red part is an average existing turning vane profile, grey is the support rib structure for modification, blue is skin covering for vane modification.

Fig. 28: Upwind section of turning vane rib modification.

Fig. 29: Downwind section of turning vane rib modification.

Fig. 30: Upwind view of turning vane proof of concept modifications in place with traverse mechanism.

Fig. 31: Downwind view of turning vane proof of concept modifications in place.

III C. Proof of Concept Results

The proof of concept turning vane modifications were measured with the same traverse mechanism as described above. Unlike the current turning vanes, there was not a significant imbalance of the measured mass flow across the vanes, at q=100 psf in the test section the mass discrepancy was 1.1%. At q=75 psf it was 3.0%, the mass loss for the modified vane is compared to the original one in Fig. 32. This decrease is likely due to the boundary layer being less prone to separation and accordingly insensitive to the traverse blockage. A photo of the traverse system behind the modified vanes is given in Fig. 33.

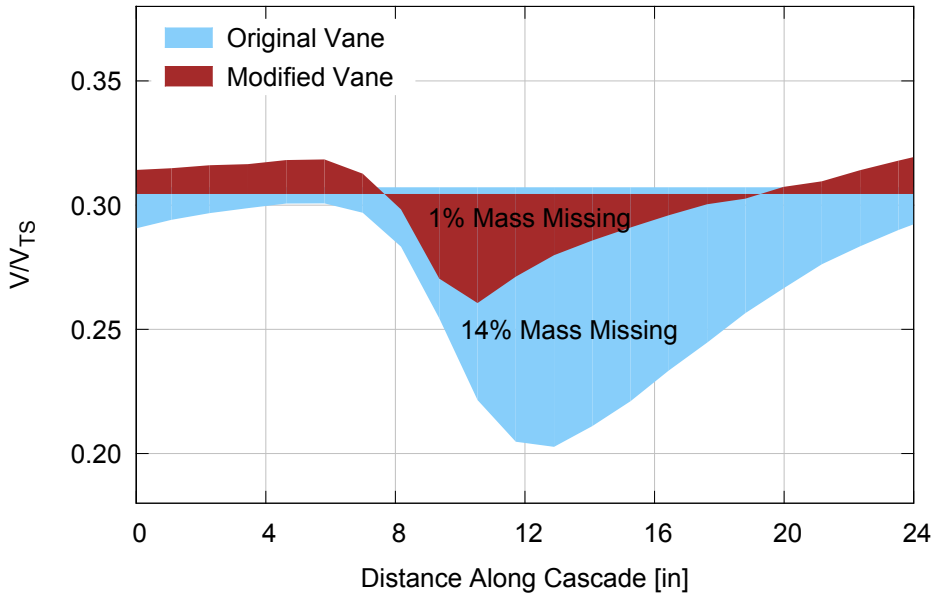

Fig. 32: Comparison of the mass lost in the turning vane measurements for the original and modified vanes at turn 2 for q=100 psf in the test section.

The shape of the flow profile is as would be expected, however, since mass is not

Fig. 33: Traverse mechanism behind proof of concept turning vanes.

conserved across the vanes a correction will be used. To correct the data, a constant will be added to the downstream measurement of total pressure. This is the value that would be most susceptible to altered flow in the turning vane cascade. The following values were added to the downwind total pressures for the current vane measurement. At q=50 psf in the test section, 1.12 psf, at q=75 psf, 1.68 psf, and at q=100 psf, 2.45 psf. For the modified vane, the total pressure constants were not as large. Their values were 0.40 psf and 0.19 psf for test section dynamic pressures of 75 psf and 100 psf, respectively. The corresponding power losses across the turning vanes and loss coefficient with and without the correction are given in Table 5 for the original turning vanes and modified ones. This analysis was carried out for one vane width.

The pressure results from these runs are given in Figs. 34 to 36. Compared to Fig. 24, the height of the dynamic pressure change is less than with the current

Table 5: Power loss and loss coefficient for turn two with and without turning vane modifications. Results with and without correction applied to downwind total pressure measurement to balance mass flow.

			q_{ts} [psf]		
		Vane	50	75	100
Power [hp]	$p_{0,measured}$	Original	57.0	106.5	148.2
		Modified	–	13.4	44.1
	$p_{0,corrected}$	Original	27.3	51.8	54.5
		Modified	–	0.1	36.9
K	$p_{0,measured}$	Original	0.475	0.488	0.415
		Modified	–	0.059	0.012
	$p_{0,corrected}$	Original	0.227	0.237	0.153
		Modified	–	0.0003	0.010

turning vanes. Showing less drag across the vane cascade.

Tuft runs were also repeated on the central modified vane. The video showed no separation for dynamic pressures up to q=100 psf in the test section. A still from the video at q=100 psf is given in Fig. 37. Eliminating separation is the main reducer in the pressure loss across the turning vane. Since this modification changed the flow from being stalled to not being stalled, a better designed airfoil would be expected to improve the power loss much less drastically.

The theoretical model shows that for test section dynamic pressures of q=50 psf and q=100 psf the expected percentage of power loss of turns one and two in relation to the entire circuit is approximately 30%. The circuit pressure measurements with the estimated correction given in Chapter II section II C. 2 give respective power loss percentages of 46% and 54% for q=50 psf and q=100 psf. Using the average of the as measured and p_t corrected values across the turning vanes, the 54% power loss

at q=100 psf could be reduced to a 21% power loss across the turning vanes with the modifications installed. Reducing the power required to run at q=100 psf at 900 RPM from 811 hp to 543 hp.

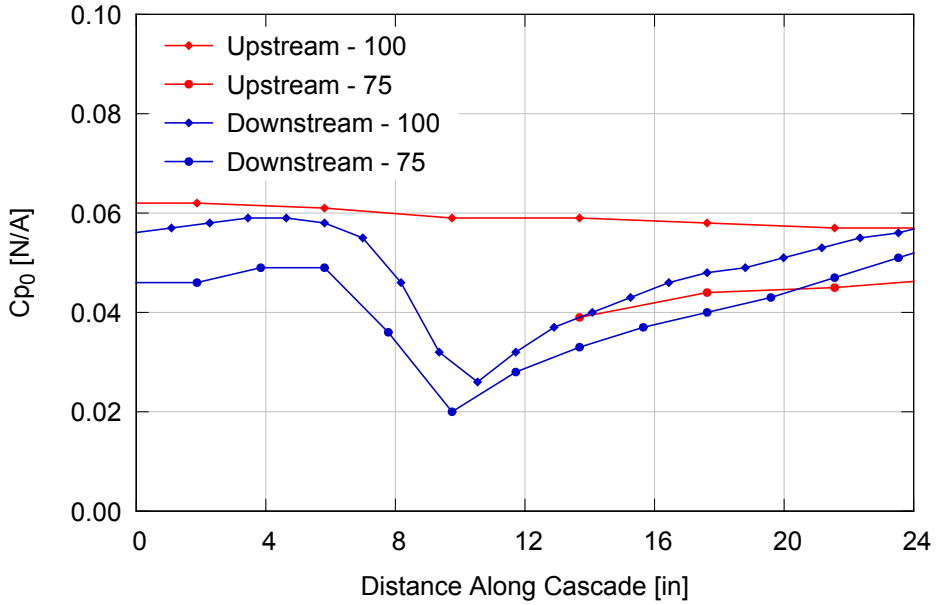

Fig. 34: Nondimensionalized total pressure upstream and downstream of modified turning vane cascade at turn two. Test section dynamic pressures of 100 and 50 psf.

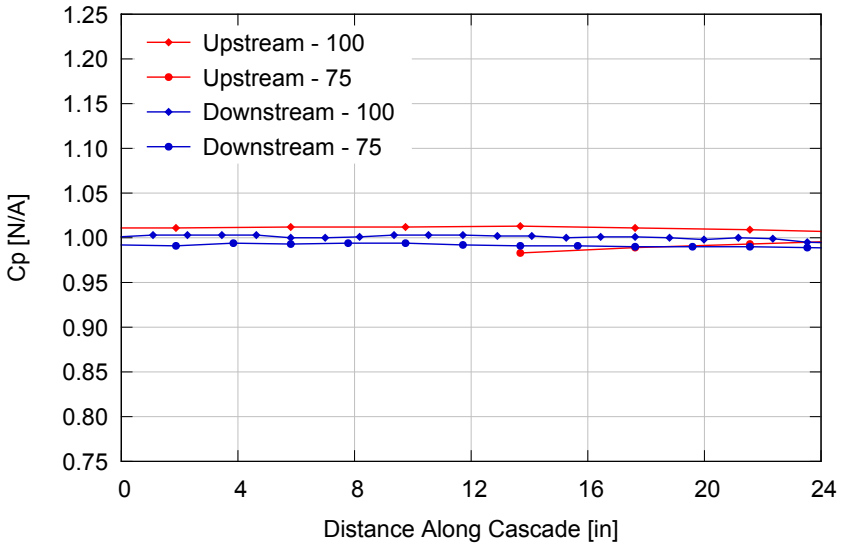

Fig. 35: Nondimensionalized static pressure upstream and downstream of modified turning vane cascade at turn two. Test section dynamic pressures of 100 and 50 psf.

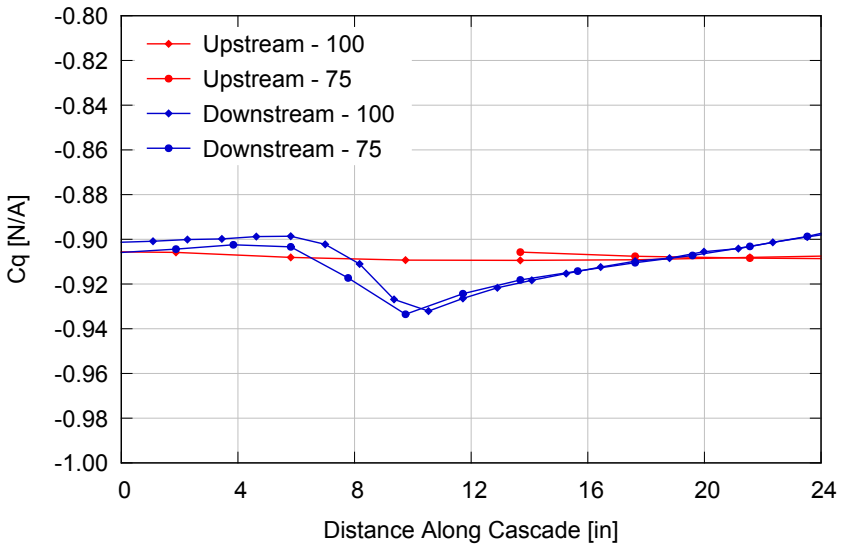

Fig. 36: Nondimensionalized dynamic pressure upstream and downstream of modified turning vane cascade at turn two. Test section dynamic pressures of 100 and 50 psf.

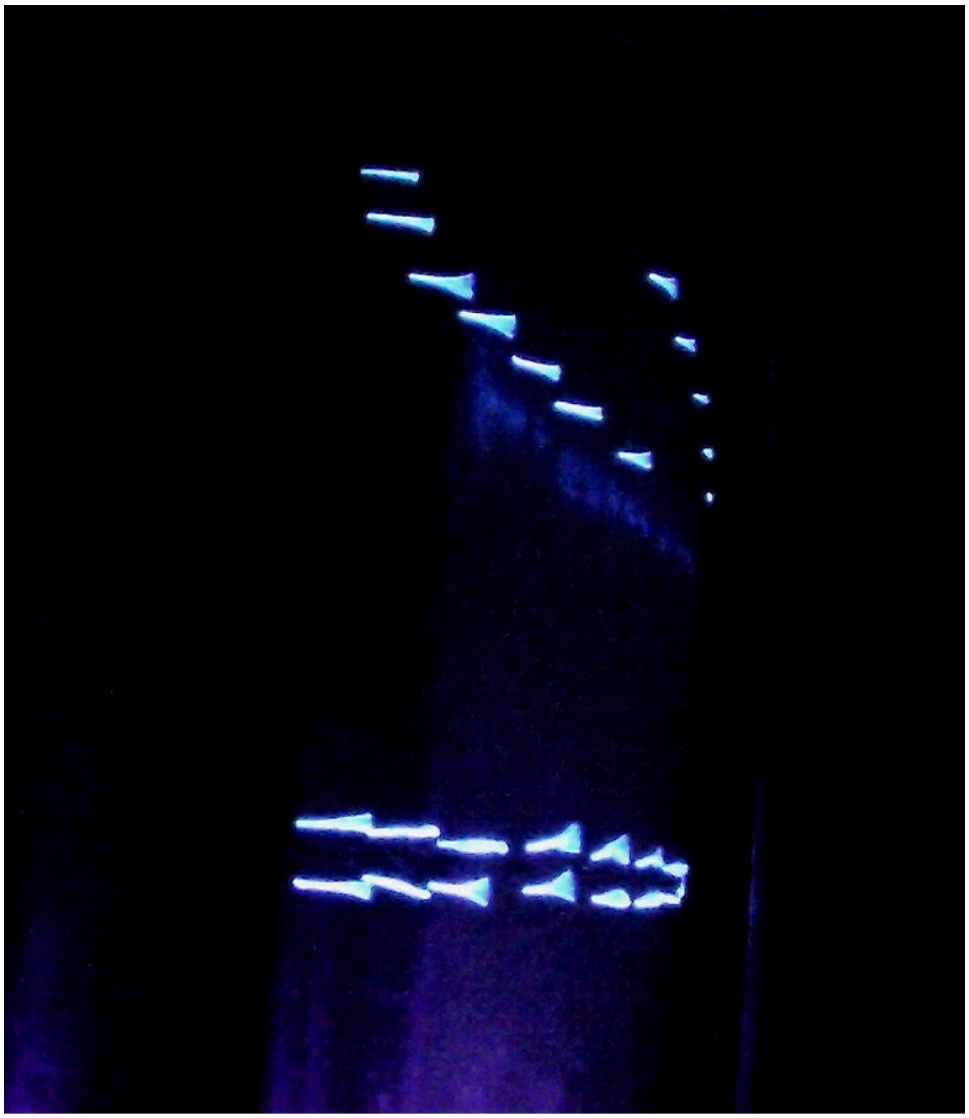

Fig. 37: Still taken from tuft run looking at the leading edge side of the modified turning vane. Test section dynamic pressure is 100 psf.

CHAPTER IV

DESIGN OF DIFFUSER INSERTS

Due to the proposed test requiring extensive modifications to the existing test section of the LSWT, a new geometry for the contraction and diffuser are needed. The design of the diffuser is the more sensitive to errors of the two and its proper design has greater implications on the power losses of the circuit. Two sources were mainly used to study the power losses of the circuit: Barlow, Rae, and Pope [6] and Eckert, Mort, and Jope [5]. These sources provided guidelines and recommendations for the diffuser design. Both of these sources emphasize the importance of careful design of the first diffuser. Since the velocity of the flow is relatively very high in this section, the potential for efficiency loss is also very high. If a diffuser is poorly designed there is the chance of intermittent or steady separation. This leads to problems including efficiency losses at that section as well as sections further downstream, surging in the test section, vibrations in the structure, and oscillatory fan loading.

The two main parameters used when designing a diffuser are the area ratio, AR, and the equivalent conical expansion angle, θ_e, which are given in Eqs. 2.25 and 2.24. General guidelines to keep the flow from separating are given in Barlow, Rae, and Pope.

> Current practice calls for a an equivalent cone angle of 3.0° or less in conjunction with typical area ratios of around 3.

The design of the new diffuser is limited by the current structure. If a single diffuser was used to expand the flow from the proposed 5 x 6 ft test section to the 12.5 ft diameter fan section, the parameters would be: $\theta_e = 4.33°$ and $AR = 4.1$ Since this is not acceptable, splitter plates must be implemented. Splitter plates divide the flow into independent parallel channels that each have a smaller equivalent cone angle. This allows the design to avoid separation but does so at the expense of increased skin friction.

IV A. Proposed Diffuser Design Geometry

The first leg of the existing primary diffuser of the LSWT begins at the exit of the test section and ends at the fan. It is approximately 46.5 ft long. The beginning is 7 x 10 ft with 1 ft chamfers, giving a cross sectional area of 68 ft^2. The exit is the start of the power section at the propeller. This cross section is a hexadecagon with a circumradius of 6.25 ft, giving an approximate area of 123 ft^2. The estimated loss coefficient is 0.030.

For the reduced test section configuration, a new diffuser was designed. It begins at the end of the 5 x 6 ft test section and ends at the fan. The design calls for two sections. The first section is 20 ft long and transitions from the rectangular cross section of the test section exit to a dodecagon. The second section is split into quadrants using two intersecting splitter plates and continues the expansion to the fan.

A MATLAB code, given in Appendix A, was written to assist with the design. The code reports the loss coefficient, power loss, area ratio, and equivalent conical

angle for a range of design input parameters. The code enables a design that minimizes power loss while meeting other design constraints. Principally, both sections should be below the recommended 3° equivalent conical angle. Small changes to a chosen design must also be made to accommodate construction concerns. The proposed design was chosen such that the equivalent conical angle for both sections would be near identical, 2.56° for the first section and 2.52° for the second. This gave the lowest value for both sections and, hopefully, will be robust to disturbances in the flow created in the test section.

In addition to the selected design, a single splitter plate design (two passages) was analyzed using this code. Although the single-splitter design gave 2% less power loss than the double splitter plate design, it also had an equivalent conical angle of 3° when both section's cone angles were matched. At this point, the area ratio for the second section was also close to 3. These are the maximum recommended values for a first diffuser given in Barlow et al. To make the design less susceptible to separation, the second splitter was added.

The MATLAB code was run for the case of a test section speed of Mach 0.5 and design inputs of varied length of the first section and area where the two sections meet. The corresponding plots can be seen in Figs. 38-40.

Since the diffuser is made from two sections, it can be seen in Fig. 38 that the minimum total loss coefficient does not correspond to the lowest power loss for the section. Fig. 39 shows that the design does not match up with the lowest possible power loss of 427 hp. Fig. 40 shows why. The diffuser design falls along the isoangle line, or where the equivalent conical angles of both sections are equal. This line gives the lowest possible equivalent conical angle for both sections. The equivalent conical

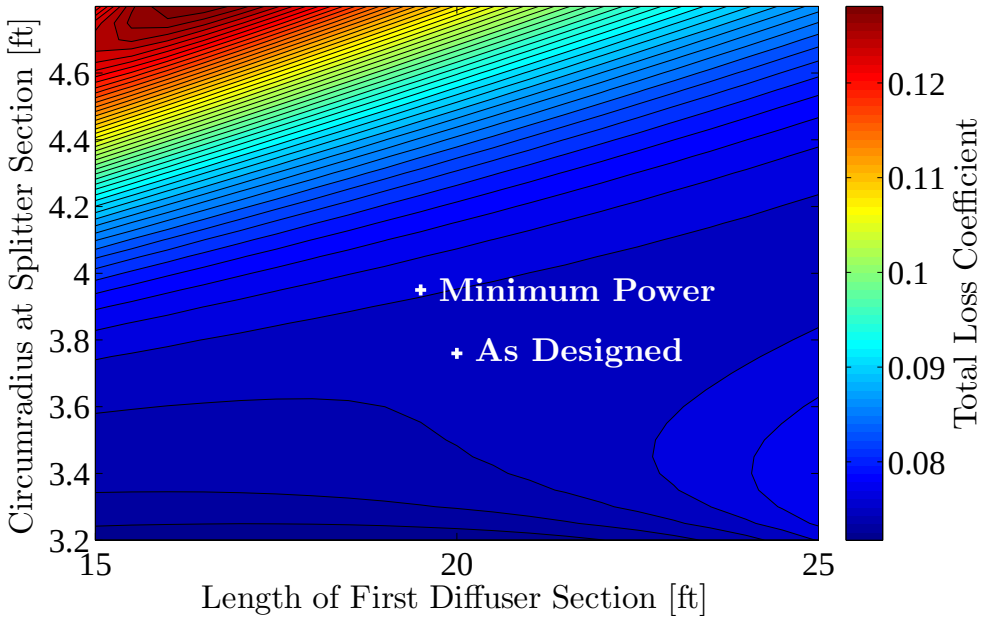

Fig. 38: Estimated total loss coefficient for the proposed diffuser design.

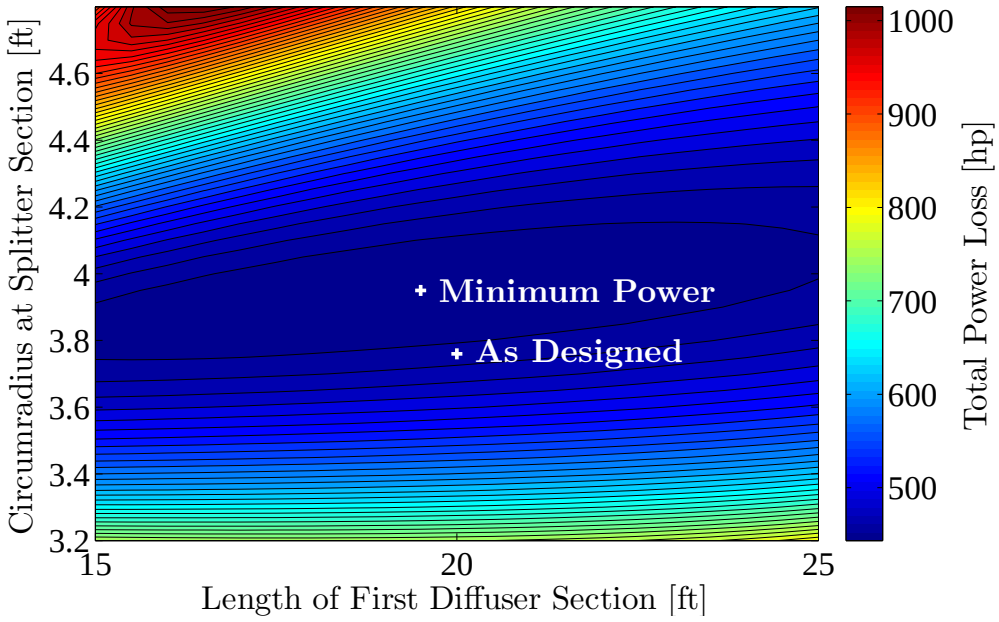

Fig. 39: Estimated total power loss for the diffuser design.

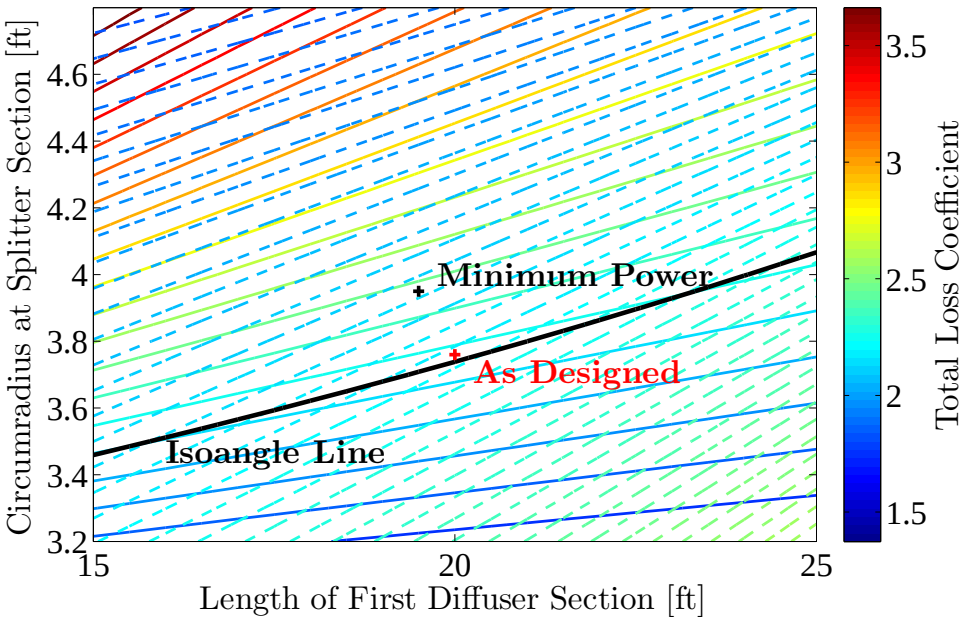

Fig. 40: Equivalent conical engles for both sections of the diffuser design. Solid lines are the first section, dashed lines are the second section.

angle as designed is 2.56° for the first section and 2.52° for the second section. The length of the first section is 20 ft and the circumradius of the dodecagonal cross section where the two halves of the diffuser meet is 3.76 ft. The total estimated power loss for the design is 442 hp, or 3.5% above the minimum power loss.

With the new test section, diffuser, and contraction, estimates for the entire circuit were made for test section Mach numbers of 0.4 and 0.5. The measured losses for corners one and two were also used to determine the losses at these speeds. The results of this model are given in Tables 6 and 7. Comparing these estimates to the estimate for the current 7 x 10 ft test section in Table 2, the locations where losses are more significant changes. For the current tunnel, at q=100 psf, the losses are more evenly spread, with 43% of the power losses occurring at the test section and primary diffuser, then turns one and two accounting for 30% of the power losses. For the 5 x 6 ft test section at M=0.4, the test section and primary diffuser make up 83% of the losses with only 11% occuring at turns one and two. This is a result of the velocities throughout the unchanged sections of the circuit being relatively low. At a reduced test section Mach number of 0.5, the velocity at the fan is M=0.106. For the current circuit, with an equivalent velocity at the fan, the test section dynamic pressure is only 57.5 psf, well below the limit of 100 psf.

The model gives an estimated power of 508.6 hp to run at M=0.4 in the new test section, and 916.3 hp to run at M=0.5. With a maximum power input to the motor of 3,000 hp and predicted efficiencies in the range of 50% to 75%, both of these goals are achievable, for an empty test section. The one unknown that would keep this goal from being reached is the stall limit for the fan blades.

Table 6: Estimated loss coefficients and power losses of the LSWT with test section and diffuser inserts at test section speed of Mach 0.4. Locations are according to Fig. 7.

Number	Type	Mach	K [NA]	P [hp]	Circuit P %
1	Constant Area Duct	0.02	0.00	0.0	0.0
2	Contraction	0.02	0.02	0.2	0.0
3	Test Section	0.40	0.02	132.5	26.1
4a	Diffuser (1^{st} section)	0.40	0.02	109.3	21.5
4b	Diffuser (2^{nd} section)	0.27	0.06	167.8	33.0
5	Power Section (Contraction)	0.09	0.00	0.2	0.0
6	Power Section (Diffuser)	0.11	0.02	8.3	1.6
7	Diffuser	0.08	0.01	2.5	0.5
8	Corner 1	0.06	0.14	41.7	8.2
9	Diffuser	0.06	0.01	0.8	0.2
10	Corner 2	0.05	0.14	27.2	5.3
11	Diffuser	0.05	0.06	4.9	1.0
12	Contraction	0.02	0.00	0.0	0.0
13	Corner 3	0.02	0.15	1.4	0.3
14	Constant Area Duct	0.02	0.00	0.0	0.0
15	Corner 4	0.02	0.15	1.4	0.3
16	Constant Area Duct	0.02	0.00	0.0	0.0
17	Screen	0.02	0.57	5.2	1.0
18	Screen	0.02	0.57	5.2	1.0
	Total			508.6	
	Total with η_f=75%			678.1	
	Total with η_f=50%			1017.2	

Table 7: Estimated loss coefficients and power losses of the LSWT with test section and diffuser inserts at test section speed of Mach 0.5. Locations are according to Fig. 7.

Number	Type	Mach	K [NA]	P [hp]	Circuit P %
1	Constant Area Duct	0.02	0.00	0.0	0.0
2	Contraction	0.02	0.02	0.3	0.0
3	Test Section	0.50	0.02	250.8	27.4
4a	Diffuser (1^{st} section)	0.50	0.02	209.7	22.9
4b	Diffuser (2^{nd} section)	0.33	0.06	307.1	33.5
5	Power Section (Contraction)	0.11	0.00	0.4	0.0
6	Power Section (Diffuser)	0.13	0.02	14.7	1.6
7	Diffuser	0.09	0.01	4.4	0.5
8	Corner 1	0.08	0.14	58.5	6.4
9	Diffuser	0.07	0.01	1.5	0.2
10	Corner 2	0.06	0.14	36.6	4.0
11	Diffuser	0.05	0.06	8.7	0.9
12	Contraction	0.02	0.00	0.0	0.0
13	Corner 3	0.02	0.15	2.5	0.3
14	Constant Area Duct	0.02	0.00	0.0	0.0
15	Corner 4	0.02	0.15	2.5	0.3
16	Constant Area Duct	0.02	0.00	0.0	0.0
17	Screen	0.02	0.57	9.3	1.0
18	Screen	0.02	0.57	9.3	1.0
	Total			916.3	
	Total with η_f=75%			1,221.7	
	Total with η_f=50%			1,832.6	

CHAPTER V

CONCLUSIONS AND RECOMMENDATIONS

The goals of this study were to determine if a test section Mach number of 0.4 and potentially 0.5 could be achieved at the LSWT with a reduced test section and redesigned contraction and diffuser. The current LSWT circuit losses were modeled using the method given in the NASA Technical Note D-8243 [5]. This model was compared to measurements made of the circuit. Tufting runs revealed separation was occurring at turns one and two. A modification to the vanes was designed and tested. This modification proved to keep the flow on the vanes from separating and to reduce the power lost at this location. A new primary diffuser section was designed for the reduced test section which would provide low power losses and decrease the chances of separation. With this new diffuser, the theoretical model was updated to predict the power required to run at M=0.4 and M=0.5.

The new model shows that to run at M=0.4 in a 5 x 6 ft test section, using the measured losses across the existing vanes at turns one and two, 509 hp must be provided to the flow. With a conservative motor and fan efficiency of 50%, 1,017 hp must be supplied to the motor. To run at M=0.5, the model predicts that 916 hp must be supplied to the flow. With a 50% efficiency, 1,833 hp must be supplied to the motor. Since the motor has a maximum input of 3,000 hp, both of these goals should be achievable for an empty test section, provided the fan blades do not reach their stall limit.

Early estimations of the power required to reach M=0.5 in the modified test section gave more marginal results. A few percent decrease in circuit pressure losses were deemed necessary. The present study concludes that the 6% to 8% decrease which would be seen from retrofitting the turning vanes in turns one and two is not required for the reduced test section experiments. The turning vane modifications, however, are recommended for normal operation of the wind tunnel. They would decrease the circuit power losses by 25% to 30% and would also result in a less turbulent test section.

An assessment of the power efficiency at motor RPM values of 900 and 1200 showed that the lower RPM value was more efficient for an empty test section. Therefore, it is recommended that the LSWT run at RPM values near this when possible. Efficiencies for test section dynamic pressures lower than 100 psf should also be made. Higher RPM values are sometimes necessary if there is significant blockage in the test section.

REFERENCES

[1] Unkown, "Wind Tunnel Building - 8," Cushing Memorial Library and Archives, Texas A&M University, College Station, Texas, 1946.

[2] Unkown, "Subsonic Wind Tunnel - 4," Cushing Memorial Library and Archives, Texas A&M University, College Station, Texas, 1958.

[3] Carr, L. W., "Progress in Analysis and Prediction of Dynamic Stall," *Journal of Aircraft*, Vol. 25, 1988.

[4] Unkown, "Wind Tunnel," Cushing Memorial Library and Archives, Texas A&M University, College Station, Texas, 1958.

[5] Eckert, W. T., Mort, K. W., and Jope, J., "Aerodynamic Design Guidelines and Computer Program for Estimation of Subsonic Wind Tunnel Performance," Technical Note D-8243, National Aeronautics and Space Administration, October 1976.

[6] Barlow, J. B., Rae Jr., W. H., and Pope, A., *Low-Speed Wind Tunnel Testing*, Wiley & Sons, Unites States of America, 1999.

[7] Sahlin, A. and Johansson, A. V., "Design of Guide Vanes for Minimizing the Pressure Loss in Sharp Bends," *Physics of Fluids*, Vol. 3, 1991.

APPENDIX A

MATLAB CODE FOR DIFFUSER DESIGN

Table of Contents


```
clc
clear all
close all
```

Design Parameters

MSr = 3.76; %circumradius of dodecagonal section dFSlength = 20; % Length of first diffuser section

```
MSr = 3.2:.05:4.8;        %circumradius of dodecagonal section
dFSlength = 15:.5:25;    % Length of first diffuser section
dSS.length = 46.5 - dFS.length;  % Length of second diffuser seciton

for j = 1:length(MSr)
    MS.r = MSr(j)

    for k = 1:length(dFSlength)

        dFS.length = dFSlength(k);
        dSS.length = 46.5 - dFS.length;
```

Constants

```
mu_0 = 3.74e-7; % reference viscosity for Sutherland's, [psf*s]
T_0 = 518.6; % reference temp for Sutherland's, [Rankine]
C = 198.6; % Sutherland's constant for air, [Rankine]
Gamma = 1.4;
R_specific = 1716.49; %Specific Gas Constant for air [ft*lbf/slug*R]

%Test Section given condidtions
TS.Mach = .5;
TS.static.Temp = 80 + 459.67; % [Rankine]
% Static pressure, equals ambient pressure (1atm) [psf]
TS.static.pressure = 2116.8;
TS.static.rho = TS.static.pressure/(R_specific * TS.static.Temp);
% Test Section Gemoetry
TS.Base = 5; % [ft]
```

```
TS.Height = 6; % [ft]
TS.Area = TS.Base*TS.Height; % [ft^2]
% Hydraulic Diameter, 4*cross sectional area / perimeter [ft]
TS.Dh = 4*TS.Area/(2*(TS.Base + TS.Height));

% Derived Values
 % common part of compressible equations
comp_const = (1+((Gamma-1).*TS.Mach.^2/2));
Astar = TS.Mach.*TS.Area.*((Gamma + 1)./(2.*comp_const))...
    .^((Gamma + 1)/(2.*(Gamma - 1)));
Total.temp = TS.static.Temp*comp_const;         % Total Temperature
Total.rho = TS.static.rho.*comp_const.^(1/(Gamma-1));   % Total density
 %speed of sound at stagnation
Total.a = sqrt(Gamma.*R_specific.*Total.temp);
 % speed of sound in moving flow at test section
TS.a = Total.a./sqrt(comp_const);
TS.U = TS.Mach.*TS.a; % Velocity in test section [ft/s]
 %Sutherland's formula
Total.mu = mu_0.*(T_0+C)./(Total.temp+C).*(Total.temp/T_0).^(1.5);
TS.q = TS.static.rho.*TS.U.^2./2;   % Test section dynamic pressure
Total.pressure = Total.rho.*R_specific.*Total.temp;
TS.RE = TS.static.rho.*TS.U.*TS.Dh./Total.mu.*(TS.Area./TS.Area)...
    .*(comp_const).^(0.76);
```

Middle Cross Section

```
 %Area of a dodecagon given circumradius
MS.Area = MS.r.^2.*12.*sin(360/12*pi()/180)./2;
% MS.Area = 42.5; %Area of second cross section
 % Length of a side of a dodecagon
MS.s = sqrt(MS.Area*4*tan(180/12*pi()/180)/12);
MS.Dh = 4*MS.Area/(12*MS.s);    % Hydraulic Diameter of a dodecagon
% MS.Dh = 7.27;   %Hydraulic Diameter
syms M
 %loop to solve for Machs at middle section for each Mach at TS
for i = 1:length(TS.Mach)
    MS.Mach(i) = real(double(solve(M^2-(Gamma+1)/(Gamma-1)...
        *(MS.Area/Astar(i)*M)^(2*(Gamma-1)/(Gamma+1)) + 2/(Gamma-1),M)));
end
MS.comp_const = 1+((Gamma-1).*MS.Mach.^2/2);
 % speed of sound ratio of middle section over TS
MS.a_ratio = sqrt(comp_const./MS.comp_const);
MS.a = TS.a.*MS.a_ratio;    % Speed of sound at middle section
MS.StaticRho = Total.rho/(MS.comp_const)^(1/(Gamma-1));
MS.U = MS.a.*MS.Mach;       % Velocity at middle section [ft/s]
MS.q = MS.StaticRho.*MS.U.^2./2;   % Middle section dynamic pressure [psf]
MS.RE = TS.static.rho.*TS.U.*MS.Dh./Total.mu.*(TS.Area./MS.Area)...
    .*(MS.comp_const).^(0.76); % Reynolds number of second section

MSq.Area = MS.Area/4;   % Area of one quadrent of second cross section
% MSq.Area = 42.5/4;    % Area of second cross section
 % Hydralic diamter of one quadrent of second cross section
MSq.Dh = 4*MSq.Area/(3*MS.s+2*MS.r);
```

```
% MSq.Dh = 3.17997;     % Hydraulic Diameter for one section of splitter
MSq.RE = TS.static.rho.*TS.U.*MSq.Dh./Total.mu.*(TS.Area./MSq.Area)...
    .*(MS.comp_const).^(0.76);
```

Fan Cross Section

```
FS.Area = 122.7; %Area of second cross section
FS.Dh = 12.5;   %Hydraulic Diameter
syms M
 %loop to solve for Machs at middle section for each Mach at TS
for i = 1:length(TS.Mach)
    FS.Mach(i) = real(double(solve(M^2-(Gamma+1)/(Gamma-1)*...
        (FS.Area/Astar(i)*M)^(2*(Gamma-1)/(Gamma+1)) + 2/(Gamma-1),M)));
end
FS.comp_const = 1+((Gamma-1).*FS.Mach.^2/2);
 % speed of sound ratio of middle section over TS
FS.a_ratio = sqrt(comp_const./FS.comp_const);
FS.a = TS.a.*FS.a_ratio;    % Speed of sound at middle section
FS.U = FS.a.*FS.Mach;       % Velocity at middle section [ft/s]
FS.StaticRho = Total.rho/(MS.comp_const)^(1/(Gamma-1));
FS.q = FS.StaticRho.*FS.U.^2./2;   % Middle section dynamic pressure [psf]
FS.RE = TS.static.rho.*TS.U.*FS.Dh./Total.mu.*(TS.Area./FS.Area)...
    .*(FS.comp_const).^(0.76); % Reynolds number of second section

FSq.Dh = 5.49876; %Hydraulic Diameter for one section of splitter
FSq.Area = 122.7/4; %Area of second cross section
FSq.RE = TS.static.rho.*TS.U.*FSq.Dh./Total.mu.*(TS.Area./FSq.Area)...
    .*(FS.comp_const).^(0.76);
```

First Section of Diffuser

Average Reynold's number of first diffuser section

```
dFS.RE = (TS.RE + MS.RE)./2;
syms f;
 % Solve for the friction coefficient at each Mach
for i = 1:length(dFS.RE)
    dFS.fric(i) = real(double(solve((log10(f*dFS.RE(i)^2)-0.8)^(-2)-f, f)));
end
dFS.AR = MS.Area/TS.Area;       % Area ratio for first section
 % Equivalent conical expansion angle
dFS.Theta_ex = radtodeg(atan((MS.Dh-TS.Dh)/(2*dFS.length)));
```

Losses of First Section

```
 %Expansion loss factor for circle
dFS.e_circle = 0.1709 - 0.117*dFS.Theta_ex + 0.0326*dFS.Theta_ex^2 ...
    +0.001078*dFS.Theta_ex^3 - 0.0009076*dFS.Theta_ex^4 ...
    -0.00001331*dFS.Theta_ex^5 + 0.00001345*dFS.Theta_ex^6;
 %Expansion loss factor for square
dFS.e_square = 0.1222156 - 0.022948*(2*dFS.Theta_ex)...
    + 0.00550704*(2*dFS.Theta_ex)^2 ...
```

```
    -0.000408644*(2*dFS.Theta_ex)^3 - 0.0000384056*(2*dFS.Theta_ex)^4 ...
    +0.00000874969*(2*dFS.Theta_ex)^5 - 0.000000365217*(2*dFS.Theta_ex)^6;
 %Expansion loss coeff for circle
dFS.ExpansionCoefficient_circle = dFS.e_circle*((dFS.AR-1)/dFS.AR)^2;
 %Expansion loss coeff for square
dFS.ExpansionCoefficient_square = dFS.e_square*((dFS.AR-1)/dFS.AR)^2;
 %Friction Loss Coefficient
dFS.FrictionCoefficient = dFS.fric./(8.*sin(degtorad(dFS.Theta_ex)))...
    .*(1-1/dFS.AR.^2);

 % Total loss coefficient for circle
dFS.TotalLossCoeff_circ = dFS.ExpansionCoefficient_circle +...
    dFS.FrictionCoefficient;
 % Total loss coefficient for square
dFS.TotalLossCoeff_sq = dFS.ExpansionCoefficient_square +...
    dFS.FrictionCoefficient;
 % Power loss for circle
dFS.PowerLoss_circ = dFS.TotalLossCoeff_circ.*TS.q.*TS.Area...
    .*TS.U.*0.00181818182;
 % Power loss for square
dFS.PowerLoss_sq = dFS.TotalLossCoeff_sq.*TS.q.*TS.Area.*TS.U.*0.00181818182;
```

Second Section of Diffuser

Average Reynold's number of first diffuser section

```
dSS.RE = (FSq.RE + MSq.RE)./2;
syms f;
for i = 1:length(dSS.RE) % Solve for the friction coefficient at each Mach
    dSS.fric(i) = real(double(solve((log10(f*dSS.RE(i)^2)-0.8)^(-2)-f, f)));
end
dSS.AR = FSq.Area/MSq.Area;       % Area ratio for first section
 % Equivalent conical expansion angle
dSS.Theta_ex = radtodeg(atan((FSq.Dh-MSq.Dh)/(2*dSS.length)));
```

Losses of First Section

```
 %Expansion loss factor for circle
dSS.e_circle = 0.1709 - 0.117*dSS.Theta_ex + 0.0326*dSS.Theta_ex^2 ...
    +0.001078*dSS.Theta_ex^3 - 0.0009076*dSS.Theta_ex^4 ...
    -0.00001331*dSS.Theta_ex^5 + 0.00001345*dSS.Theta_ex^6;
 %Expansion loss factor for square
dSS.e_square = 0.1222156 - 0.022948*(2*dSS.Theta_ex) +...
    0.00550704*(2*dSS.Theta_ex)^2 ...
    -0.000408644*(2*dSS.Theta_ex)^3 - 0.0000384056*(2*dSS.Theta_ex)^4 ...
    +0.00000874969*(2*dSS.Theta_ex)^5 - 0.000000365217*(2*dSS.Theta_ex)^6;
 %Expansion loss coeff for circle
dSS.ExpansionCoefficient_circle = dSS.e_circle*((dSS.AR-1)/dSS.AR)^2;
 %Expansion loss coeff for square
dSS.ExpansionCoefficient_square = dSS.e_square*((dSS.AR-1)/dSS.AR)^2;

dSS.FrictionCoefficient = dSS.fric./(8.*sin(degtorad(dSS.Theta_ex)))...
    .*(1-1/dSS.AR.^2);  %Friction Loss Coefficient
```

```
dSS.TotalLossCoeff_circ = dSS.ExpansionCoefficient_circle +...
    dSS.FrictionCoefficient; % Total loss coefficient for circle
dSS.TotalLossCoeff_sq = dSS.ExpansionCoefficient_square +...
    dSS.FrictionCoefficient;   % Total loss coefficient for square
dSS.PowerLoss_circ = dSS.TotalLossCoeff_circ.*MS.q.*MS.Area...
    .*MS.U.*0.00181818182;    % Power loss for circle
dSS.PowerLoss_sq = dSS.TotalLossCoeff_sq.*MS.q....
    *MS.Area.*MS.U.*0.00181818182;        % Power loss for square
```

Summary of simulation

```
first_circ(j,k) = dFS.PowerLoss_circ;% Power loss for first section (circle)
first_sq(j,k) = dFS.PowerLoss_sq;
second_circ(j,k) = dSS.PowerLoss_circ;% Power loss for second section (circle)
second_sq(j,k) = dSS.PowerLoss_sq;
 % Total power loss for diffuser (circle)
Total_circ(j,k) = first_circ(j,k) + second_circ(j,k);
Total_sq(j,k) = first_sq(j,k) + second_sq(j,k);

% First and second section loss coefficients
FS_Coeff_circ(j,k) = dFS.TotalLossCoeff_circ;
FS_Coeff_sq(j,k) = dFS.TotalLossCoeff_sq;
SS_Coeff_circ(j,k) = dSS.TotalLossCoeff_circ;
SS_Coeff_sq(j,k) = dSS.TotalLossCoeff_sq;
TotalCoeff_sq(j,k) = dFS.TotalLossCoeff_sq + dSS.TotalLossCoeff_sq;
TotalCoeff_circ(j,k) = dFS.TotalLossCoeff_circ + dSS.TotalLossCoeff_circ;

% Area ratios and equivalent conical expansions for both sections
first_AR(j,k) = dFS.AR;
second_AR(j,k) = dSS.AR;
first_angle(j,k) = dFS.Theta_ex;
second_angle(j,k) = dSS.Theta_ex;

    end
end

% Save output
save('diffuser_results.mat');
```

Plots

```
close all
fontsize = 18;
papesz = [8,5];
papepos = [-1.5,0,9.5,5];

% Plot power loss
figure('Name','Power Plot','units','normalized','outerposition'...
    ,[0 0.666 .333 .333])
set(gcf,'PaperSize', papesz);
set(0,'DefaultAxesFontName', 'Times New Roman')
```

```
set(0,'DefaultAxesFontSize', fontsize)
contourf(dFSlength,MSr,Total_sq,50)
xlabel('Length of First Diffuser Section [ft]'...
    ,'Interpreter','Latex','FontSize',fontsize)
ylabel('Circumradius at Splitter Section [ft]'...
    ,'Interpreter','Latex','FontSize',fontsize)
hold on
plot(20,3.76,'w+','linewidth',2)
plot(19.5,3.95,'w+','LineWidth',2)
text('Interpreter','latex','Position',[20.25,3.76]...
    , 'String','\bf As Designed', 'Color', 'w','FontSize',fontsize);
text('Interpreter','latex','Position',[19.75,3.95]...
    , 'String','\bf Minimum Power', 'Color', 'w','FontSize',fontsize);
t = colorbar;
set(get(t,'ylabel'),'String', 'Total Power Loss [hp]'...
    ,'Interpreter','Latex','FontSize',fontsize);
set(gcf,'paperunits','inches')
set(gcf,'papersize',papesz)
set(gcf,'paperposition',papepos)
print('-dpdf','DiffPlot_Power')

% Plot loss coefficient
figure('Name','Loss Coefficient Plot','units'...
    ,'normalized','outerposition',[0 0.333 .333 .333])
set(gcf,'PaperSize', papesz);
set(0,'DefaultAxesFontName', 'Times New Roman')
set(0,'DefaultAxesFontSize', fontsize)
contourf(dFSlength,MSr,TotalCoeff_sq,50)
xlabel('Length of First Diffuser Section [ft]'...
    ,'Interpreter','Latex','FontSize',fontsize)
ylabel('Circumradius at Splitter Section [ft]'...
    ,'Interpreter','Latex','FontSize',fontsize)
hold on
plot(20,3.76,'w+','linewidth',2)
plot(19.5,3.95,'w+','LineWidth',2)
text('Interpreter','latex','Position',[20.25,3.76]...
    , 'String','\bf As Designed', 'Color', 'w','FontSize',fontsize);
text('Interpreter','latex','Position',[19.75,3.95]...
    , 'String','\bf Minimum Power', 'Color', 'w','FontSize',fontsize);
t = colorbar;
set(get(t,'ylabel'),'String', 'Total Loss Coefficient'...
    ,'Interpreter','Latex','FontSize',fontsize);
set(gcf,'paperunits','inches')
set(gcf,'papersize',papesz)
set(gcf,'paperposition',papepos)
print('-dpdf','DiffPlot_Coeff')

% Plot equivalent conical angle
figure('Name','Design Parameters: Equivalent Conical Angle [deg]'...
    ,'units','normalized','outerposition',[0 0 .333 .333])
set(gcf,'PaperSize', papesz);
set(0,'DefaultAxesFontName', 'Times New Roman')
set(0,'DefaultAxesFontSize', fontsize)
contour(dFSlength,MSr,first_angle,20,'LineWidth',1.5)
```

```
xlabel('Length of First Diffuser Section [ft]'...
    ,'Interpreter','Latex','FontSize',fontsize)
ylabel('Circumradius at Splitter Section [ft]'...
    ,'Interpreter','Latex','FontSize',fontsize)
hold on
contour(dFSlength,MSr,second_angle,40,'LineStyle','--','LineWidth',1.5)
contour(dFSlength,MSr,(first_angle-second_angle)...
    ,[0;0],'LineWidth',2.5,'Color','k')
text('Interpreter','latex','Position',[16,3.46]...
    , 'String','\bf Isoangle Line', 'Color', 'k','FontSize',fontsize);
plot(20,3.76,'r+','linewidth',2)
text('Interpreter','latex','Position',[20.25,3.7]...
    , 'String','\bf As Designed', 'Color', 'r','FontSize',fontsize);
plot(19.5,3.95,'k+','LineWidth',2)
text('Interpreter','latex','Position',[19.75,4]...
    , 'String','\bf Minimum Power', 'Color', 'k','FontSize',fontsize);
t = colorbar;
set(get(t,'ylabel'),'String', 'Total Loss Coefficient'...
    ,'Interpreter','Latex','FontSize',fontsize);
set(gcf,'paperunits','inches')
set(gcf,'papersize',papesz)
set(gcf,'paperposition',papepos)
print('-dpdf','DiffPlot_Angle')
```

Published with MATLAB® 8.0